

Double-exchange theory of ferroelectric polarization in orthorhombic manganites with twofold periodic magnetic texture

I. V. Solovyev^{1,2,*} and S. A. Nikolaev²

¹*Computational Materials Science Unit,
National Institute for Materials Science,*

1-2-1 Sengen, Tsukuba, Ibaraki 305-0047, Japan

²*Department of Theoretical Physics and Applied Mathematics,
Ural Federal University, Mira str. 19, 620002 Ekaterinburg, Russia*

(Dated: March 13, 2013)

Abstract

We argue that many aspects of improper ferroelectric activity in manganites with the $Pbnm$ and $P2_1nm$ orthorhombic structure can be rationalized by considering the limit of infinite intra-atomic splitting between the majority- and minority-spin states (or the double exchange limit), which reduces the problem to the analysis of a spinless double exchange (DE) Hamiltonian. We apply this strategy to the low-energy model, derived from the first-principles electronic structure calculations, and combine it with the Berry-phase theory of electric polarization. We start with the simplest two-orbital model, describing the behavior of the e_g bands, and apply it to the E -type antiferromagnetic (AFM) phase, which in the DE limit effectively breaks up into one-dimensional zigzag chains. We derive an analytical expression for the electronic polarization (\mathbf{P}^{el}) and explain how it depends on the orbital ordering and the energy splitting Δ between e_g states. Then, we evaluate parameters of this model for the series of manganites. For these purposes we start from a more general five-orbital model for all Mn $3d$ bands and construct a new downfolded model for the e_g bands. From the analysis of these parameters, we conclude that the behavior of \mathbf{P}^{el} in realistic manganites always corresponds to the limit of large Δ . This property holds for all considered compounds even in the local-density approximation, which typically underestimates Δ . We further utilize this property in order to derive an analytical expression for \mathbf{P}^{el} in a general two-fold periodic magnetic texture, based on the five-orbital model and the perturbation-theory expansion for the Wannier functions in the first order of $1/\Delta$. This expression explains the functional dependence of \mathbf{P}^{el} on the relative directions of spins. Furthermore, it suggests that \mathbf{P}^{el} is related to the asymmetry of the transfer integrals, which should simultaneously have symmetric and antisymmetric components. Finally, we explain how the polarization can be switched between orthorhombic directions \mathbf{a} and \mathbf{c} by inverting the zigzag AFM texture in every second \mathbf{ab} plane. We argue that this property is generic and can be realized even in the twofold periodic texture.

I. INTRODUCTION

The multiferroic materials (or multiferroics), where ferroelectricity coexists with some long-range magnetic order, have attracted a great deal of attention.¹ A very special class of multiferroics is improper ferroelectrics. In the latter case, the ferroelectric (FE) polarization not only coexists, but can be induced by the magnetic order. The improper ferroelectrics are expected to display a strong magneto-electric coupling, which is extremely important for practical applications. For instance, because of such coupling, the FE polarization can be efficiently controlled by the magnetic field, while the magnetization can be controlled by the electric field. From a technological point of view, the ultimate goal is to find materials with the large FE polarization, which would be coupled to the magnetic texture at maximally possible temperature (meaning that the magnetic transition temperature should be also high).

Manganites, crystalizing in the orthorhombic $Pbnm$ and $P2_1nm$ structure, are regarded as one of the key multiferroic materials. Despite low magnetic transition temperature (typically, less than 40 K) and modest values of the FE polarization (less than $1 \mu\text{C}/\text{cm}^2$), which have been achieved so far,² they have all essential ingredients to be called improper ferroelectrics. Namely, the appearance of ferroelectricity coincides with some complex magnetic ordering. Moreover, the possibility of switching the electric polarization by the magnetic fields has been directly demonstrated experimentally.³ Therefore, these materials are fundamentally important and are typically used as a playground for testing various theories and models of multiferroicity.

Nevertheless, the theoretical understanding of improper ferroelectricity in these compounds is still rather controversial and there is no unique view on the origin of this effect. First, all multiferroic manganites are rather artificially divided in two groups:

- (i) the systems with the twofold periodic E -type antiferromagnetic (AFM) texture (such as HoMnO_3 and YMnO_3), where the FE activity is attributed to the nonrelativistic exchange striction,^{4,5} and
- (ii) the rest of the systems, with more general magnetic periodicity, where the FE activity is believed to be due to the relativistic spin-orbit (SO) interaction and the magnetic texture itself is ascribed to the spin spiral.⁶ The typical example of such systems is

TbMnO₃, which has nearly fourfold periodic magnetic texture.

This point was rationalized in the previous publications of one of the authors (Ref. 7 and 8), where it was argued that there is no conceptual difference between twofold periodic and other multiferroic manganites. The relativistic SO interaction plays an equally important role in both cases: as it deforms the *E*-type AFM state in the direction of the spin spiral, it will also deform the spin spiral and form a more general spatially inhomogeneous magnetic state. Thus, the ground state of multiferroic manganites will be neither the collinear *E*-state nor the homogeneous spin spiral. The relativistic SO interaction is essential for producing this inhomogeneity. However, the FE polarization itself is a nonrelativistic quantity in the sense that, for a given inhomogeneous distribution of spins, the appearance of the FE polarization can be described by nonrelativistic theories.

Another group of controversies is related to the question: How to calculate the polarization and what is the main contribution to it? Most of model calculations rely on the purely ionic picture, where the noncentrosymmetric distribution of spins gives rise to noncentrosymmetric atomic displacements. Then, the polarization is evaluated in the framework of the point charge model.^{4,9} On the other hand, all modern first-principles calculations of the FE polarization are based on the Berry-phase theory.^{10,11} Besides ionic polarization, the Berry-phase theory prescribes the existence of an electronic term. The latter can be expressed through the Wannier functions and is reduced to the ionic polarization only if the Wannier functions are fully localized at the atomic sites. In this sense, the deviation from the ionic picture is a measure of itineracy of the system. Moreover, unlike the ionic contribution, the electronic polarization can be finite even in the centrosymmetric crystal structure, provided that the inversion symmetry is broken by a magnetic order. Thus, the Berry-phase theory excellently suits for improper ferroelectrics. The first-principles calculations show that the electronic polarization can be as large as or even exceed the ionic contribution.⁵ Nevertheless, the physical meaning of this effect is still rather obscure and the electronic polarization is largely ignored in model calculations of multiferroic manganites.

The purpose of this work is to make a bridge between first-principle electronic structure calculations and models of the FE polarization. Our main message is that the electronic polarization is important and cannot be ignored. In the model calculations, it can be described by some “superexchange type” theories, similar to interatomic magnetic interactions.^{12,13} On the other hand, in the first-principles calculations, one should pay a special attention to the

relative direction of the electronic and ionic polarization: because of additional approximations, results of theoretical structural optimization do not necessarily guarantee the correct answer to this question.

Our analysis will be based on results of two previous works (Refs. 7 and 8), where

- (i) A realistic low-energy model for the Mn $3d$ bands of manganites was constructed on the basis of first-principles electronic structure calculations in the local-density approximation (LDA);
- (ii) This model was applied for the search of the magnetic ground state of orthorhombic manganites;
- (iii) The model calculations were supplemented with the Berry-phase theory for the analysis of the FE polarization and its dependence on the form of the magnetic ground state.

In this work we will further rationalize the story. First, we will show that the behavior of the FE polarization can be well described in the framework of the double exchange (DE) theory.¹⁴ The definition of the DE Hamiltonian will be given in Sec. II. Particularly, we will show that with the proper definition of the DE model, which should include effects of orbital polarization of Coulombic origin, one can reproduce, even quantitatively, the values of FE polarization obtained in a more general mean-field Hartree-Fock (HF) calculations for the low-energy model. Then, we will introduce an analytically solvable model for the e_g electrons in the single zigzag chain (Sec. III A) and argue that, besides double exchange, the behavior of electronic polarization in realistic manganites always corresponds to the limit of large intra-atomic energy splitting Δ between e_g states (Sec. III B). It will allow us to further generalize our story and derive an analytical expression for the electronic polarization in an arbitrary twofold periodic magnetic texture, based on the perturbation theory expansion for the Wannier functions in the first order of $1/\Delta$ (Sec. III C). The idea itself has some similarities with the superexchange theory of interatomic magnetic interactions.^{12,13} This analytical expression nicely explains the behavior of electronic polarization in the low-energy model as well as in the more general first-principles calculations. It also provides a good quantitative estimate for the polarization. In Sec. III D, we will present a critical analysis of relative directions of electronic and ionic polarizations in the experimental and theoretically optimized $P2_1nm$ structures of YMnO_3 . Then, in Sec. III E, we will explain how the electronic

polarization can be manipulated by changing the magnetic texture. Finally, in Sec. IV, we draw our conclusions.

II. BASIC IDEA AND APPROXIMATIONS

The starting point of our work is that the main electronic and magnetic properties of multiferroic manganites can be described reasonably well by the one-electron Hamiltonian:

$$\hat{H}_{ij}^{\text{MF}} = \hat{t}_{ij} + \hat{\mathcal{V}}_i \delta_{ij}, \quad (1)$$

which is constructed in the basis of Wannier orbitals for the Mn 3d bands. In this notations, the matrix \hat{t}_{ij} has site-diagonal ($i = j$) and off-diagonal ($i \neq j$) elements: the former describes the crystal-field effects, while the latter stands for transfer integrals. We do not consider explicitly the relativistic spin-orbit (SO) interaction. More specifically, it is assumed that the SO interaction is important for specifying the directions of spins in some noncollinear magnetic texture. However, it is unimportant for calculations of the FE polarization itself, provided that the directions of spins are known and the corresponding magnetic texture can be described by appropriate rotations of the mean-field potentials $\hat{\mathcal{V}}_i$, which will be specified below. Therefore, the matrix \hat{t}_{ij} does not depend on the spin-indices, $s(s') = \uparrow$ or \downarrow , and can be presented in the form $\hat{t}_{ij} = \|t_{ij}^{mm'} \delta_{ss'}\|$. In the more general five-orbital model, that we consider, the indices m and m' have the following order: $m(m') = xy, yz, 3z^2 - r^2, zx$, or $x^2 - y^2$. In the two-orbital model, constructed only for the e_g bands, the indices m and m' run over $3z^2 - r^2$ and $x^2 - y^2$. $\hat{\mathcal{V}}_i$ in Eq. (1) is the self-consistent one-electron potential, which is constructed using parameters of effective Coulomb interactions and the density matrix for the Mn 3d states. Generally, $\hat{\mathcal{V}}_i$ depends on both spin and orbital indices.

In practice, the electronic low-energy model can be derived from the first-principles electronic structure calculations, starting from the local-density approximation (LDA).¹⁵ The construction of the model can be formulated rather rigorously in the basis of Wannier orbitals for the Mn 3d bands. Then, \hat{t}_{ij} is identified with the matrix elements of the LDA Hamiltonian in the Wannier basis. Thus, without $\hat{\mathcal{V}}_i$, the parameters \hat{t}_{ij} describe the LDA electronic structure for the Mn 3d bands. The parameters of effective Coulomb interactions for the Mn 3d bands can be derived, also in the Wannier basis, using constrained random-phase approximation and/or the constrained LDA approach. For details, the reader

is referred to the review article (Ref. 15). Then, the model can be solved in the mean-field HF approximation, which gives us the potentials $\hat{\mathcal{V}}_i$.¹⁵

After the solution, the FE polarization can be obtained by applying the Berry-phase theory.^{10,11} Namely, the FE polarization is divided into the ionic (ion) and electronic (el) parts:

$$\mathbf{P} = \mathbf{P}^{\text{ion}} + \mathbf{P}^{\text{el}}.$$

The ionic term reflects the non-centrosymmetry of the crystal structure itself and is associated with the displacements ($\Delta\boldsymbol{\tau}_i$) of ionic charges (Z_i) away from the centrosymmetric positions:

$$\mathbf{P}^{\text{ion}} = \frac{1}{V} \sum_i Z_i \Delta\boldsymbol{\tau}_i, \quad (2)$$

where V is the primitive cell volume. The electronic term reflects the fact of the inversion symmetry breaking in the form of the wavefunctions, obtained from the solution of quantum-mechanical Schrödinger equations. It incorporates the effects of the magnetic inversion symmetry breaking and can take place even for centrosymmetric crystalline systems, provided that the inversion symmetry is broken by magnetic or some other electronic degrees of freedom. The electronic term can be computed in the reciprocal space, by using the formula of King-Smith and Vanderbilt:¹⁰

$$\mathbf{P}^{\text{el}} = -\frac{ie}{(2\pi)^3} \sum_{n=1}^M \int_{\text{BZ}} \langle n\mathbf{k} | \nabla_{\mathbf{k}} | n\mathbf{k} \rangle d\mathbf{k}, \quad (3)$$

where $|n\mathbf{k}\rangle$ is the cell periodic wavefunction, the summation runs over the occupied bands (n), the \mathbf{k} -space integration goes over the first Brillouin zone, and $-e$ ($e > 0$) is the electron charge. In practical calculations, Eq. (3) is replaced by a discrete grid formula.¹¹ Eq. (3) can be also rewritten in terms of the Wannier function (w_n), constructed from $|n\mathbf{k}\rangle$ in the real space:¹⁰

$$\mathbf{P}^{\text{el}} = -\frac{e}{V} \sum_{n=1}^M \int \mathbf{r} |w_n(\mathbf{r})| d\mathbf{r}. \quad (4)$$

In all these equations, it is understood that \mathbf{P} is the *change* of the polarization, obtained in the process of adiabatic lowering of the inversion symmetry.¹¹ Moreover, the contribution of the low-energy bands (in our case, the Mn 3d bands) is accounted by \mathbf{P}^{el} . Therefore, the contribution of all other occupied states, which are not included to the low-energy model, should be described (at least, approximately) by \mathbf{P}^{ion} . Then, since the oxygen 2p band is

fully occupied, it is reasonable to take $Z_{\text{O}} = -2e$, which corresponds to the formal valence state of O^{2-} . On the other hand, all valence states of the rare-earth (RE) ions are empty. This should correspond to $Z_{\text{RE}} = 3e$. In the noncentrosymmetric $P2_1nm$ structure, the Mn sites do not contribute to \mathbf{P}^{ion} .⁸ Therefore, the parameter Z_{Mn} is not important for our purposes.

In the previous publications, this procedure was applied to the series of orthorhombic manganites. Particularly, the behavior of parameters of the low-energy model, derived from the first-principles electronic structure calculations, was discussed in Ref. 16. An example of such parameters for YMnO_3 can be found in Supplemental Material of Ref. 8. The properties of the magnetic ground state, obtained from the solution of the low-energy model in the HF approximation, and corresponding behavior of the FE polarization were considered in Refs. 7 and 8. Note that a scaling factor was missing in the calculations of the FE polarization reported in Ref. 7. This error was corrected in Ref. 8.

As far as the FE polarization is concerned, the low-energy model reproduces results of the first-principles electronic structure calculations (Refs. 5, 17, and 18) on a good semi-quantitative level. Moreover, the low-energy model was very helpful in clarifying details of the noncollinear magnetic ground state, which can be realized in orthorhombic manganites, namely: (i) the canting of spins and magnetic origin of the twofold periodic phase;^{7,8} (ii) deformation of the spin-spiral texture, yielding FE activity in both two- and fourfold periodic systems;⁷ (iii) the absence of the magnetic inversion symmetry breaking in systems with odd magnetic periodicity.⁷

In this work, we will further rationalize the story by considering the DE limit for the FE polarization.

Let us start with the ferromagnetic (FM) state, where each $\hat{\mathcal{V}}_i$ is diagonal with respect to the spin indices,

$$\hat{\mathcal{V}}_i = \begin{pmatrix} \hat{\mathcal{V}}_i^{\uparrow} & 0 \\ 0 & \hat{\mathcal{V}}_i^{\downarrow} \end{pmatrix},$$

and $\hat{\mathcal{V}}_i^{\uparrow,\downarrow}$ are the 5×5 matrices in the orbital subspace. The states with $s = \uparrow$ are occupied by four electrons and the ones with $s = \downarrow$ are empty. Then, $\hat{\mathcal{V}}_i^{\downarrow}$ can be identically presented in the form: $\hat{\mathcal{V}}_i^{\downarrow} = \Delta_{\text{ex}} + \Delta\hat{\mathcal{V}}_i^{\downarrow}$, where Δ_{ex} is the intra-atomic exchange splitting between centers of gravity of the majority (\uparrow) and minority (\downarrow) spin states, and $\Delta\hat{\mathcal{V}}_i^{\downarrow}$ describes the orbital splitting of unoccupied \downarrow -spin states. Moreover, four $3d$ electrons obey Hund's first

rule, which tend to form the state with the maximal spin $S = 2$. Therefore, besides on-site Coulomb repulsion (U), Δ_{ex} will contain a large contribution, being proportional to the local magnetic moment ($2S$) and the intra-atomic exchange coupling (J_{H}). This is the main reason why for many applications Δ_{ex} can be treated as the largest physical parameter, and the DE limit corresponds to the extreme situation where $\Delta_{\text{ex}} \rightarrow \infty$.¹⁴ On the other hand, the splitting of unoccupied \downarrow -spin states is considerably weaker. For example, in the HF approximation, it is caused by relatively small nonsphericity of the Coulomb potential.

Therefore, when $\Delta_{\text{ex}} \rightarrow \infty$, the details of (finite) splitting of the \downarrow -spin states become unimportant and our first approximation is to replace $\Delta\hat{\mathcal{V}}_i^\downarrow$ by $\hat{\mathcal{V}}_i^\uparrow$. It allows us to present $\hat{\mathcal{V}}_i$ in the following form:

$$\hat{\mathcal{V}}_i \approx \hat{\mathcal{V}}_i^\uparrow + \begin{pmatrix} 0 & 0 \\ 0 & \Delta_{\text{ex}} \end{pmatrix}, \quad (5)$$

where the orbital-dependent part ($\hat{\mathcal{V}}_i^\uparrow$) does not depend on the spin indices and the spin-dependent part does not depend on the orbital ones. Therefore, spin and orbital transformations of Eq. (5) can be treated separately.

A typical example, illustrating the structure of the atomic $3d$ level splitting by the Coulomb and exchange potentials in the low-energy model, is shown in Fig. 1. Typical values of Δ_{ex} in manganites are about 4.5 eV, while the splitting of the \downarrow -spin states is about 1.7 eV. The difference is not extremely large. However, as we will see in a moment, it is sufficient to justify the use of the DE limit for the FE polarization.

As the next step, let us consider an arbitrary magnetic texture, where the directions of spin (\mathbf{e}_i) at each site of the lattice are specified by the combinations of polar (θ_i) and azimuthal (ϕ_i) angles: $\mathbf{e}_i = (\cos \phi_i \sin \theta_i, \sin \phi_i \sin \theta_i, \cos \theta_i)$. Corresponding electronic structure can be generated by the unitary transformation of Eq. (5), using spin-rotation matrices:

$$\hat{\mathcal{V}}_i \rightarrow \hat{U}(\theta_i, \phi_i) \hat{\mathcal{V}}_i \hat{U}^\dagger(\theta_i, \phi_i), \quad (6)$$

where

$$\hat{U}(\theta_i, \phi_i) = \begin{pmatrix} \cos \frac{\theta_i}{2} & \sin \frac{\theta_i}{2} e^{-i\phi_i} \\ -\sin \frac{\theta_i}{2} e^{i\phi_i} & \cos \frac{\theta_i}{2} \end{pmatrix}.$$

Here, it is assumed that the angles (θ_i, ϕ_i) are specified by magnetic interactions in the system (for the form of the optimized magnetic textures, the reader is referred to Refs. 7 and 8) and the one-electron potential for an arbitrary direction of spin can be obtained by

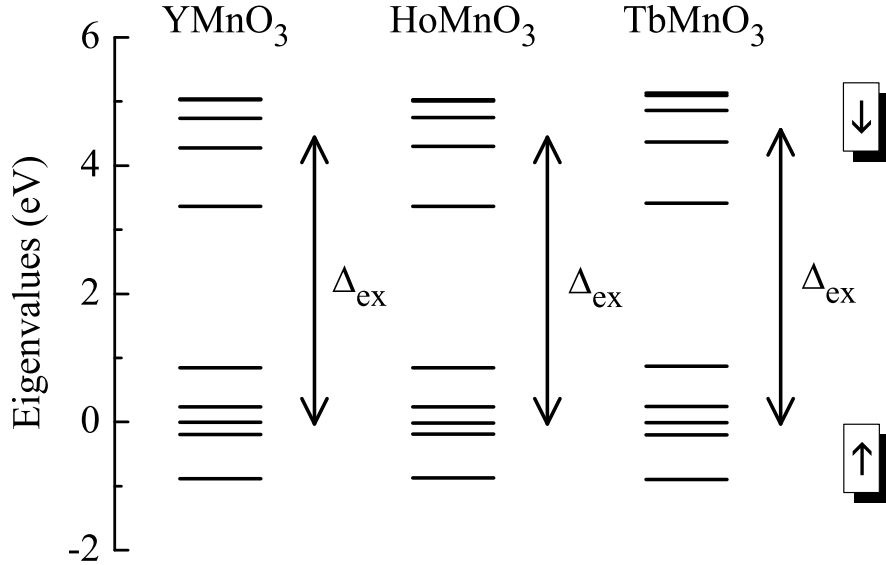


FIG. 1. Eigenvalues of the Hartree-Fock potential, as obtained in the low-energy model for the ferromagnetic phase of YMnO₃, HoMnO₃, and TbMnO₃ (results of Refs. 7 and 8 for the experimental *Pbnm* structure). Δ_{ex} is the intra-atomic splitting between centers of gravity of the majority (\uparrow) and minority (\downarrow) spin states.

using rigid spin rotations [Eq. (6)] without additional self-consistency. This is a very good approximation in the case of manganites, because:

- (i) Due to the strong Hund's coupling, the local spin magnetization will always tend to stay in the saturated state. Therefore, the absolute value of this magnetization will only weakly depend on the direction of spins at other magnetic sites.
- (ii) The orbital configuration is rigidly fixed by the Jahn-Teller (JT) distortion and practically does not depend on the type of the spin texture. For example, the energy splitting of the e_g states, caused by the JT distortion, is about 1.5 eV, while typical strength of interatomic exchange interactions is of the order of several meV.¹⁶ The exchange interactions can be additionally optimized by means of the orbital reconstruction, which works against the JT splitting.¹³ However, the possible energy gain, caused by this reconstruction (typically, of the order of the exchange interactions themselves) is much smaller than the energy of the JT distortion. Thus, the orbital reconstruction does not occur.

The next step is to transform Eq. (6) to the local coordinate frame, corresponding to the z direction of magnetization at each site of the lattice. It leads to the following transformation of the transfer integrals:

$$\hat{t}_{ij} \rightarrow \hat{U}^\dagger(\theta_i, \phi_i) \hat{t}_{ij} \hat{U}(\theta_j, \phi_j).$$

Then, taking the limit $\Delta_{\text{ex}} \rightarrow \infty$, we obtain the well known DE model:

$$\hat{H}_{ij}^{\text{DE}} = \xi_{ij} \hat{t}_{ij} + \hat{\mathcal{V}}_i^\dagger \delta_{ij}, \quad (7)$$

which formulated in the subspace of the \uparrow -spin states, in the local coordinate frame.¹⁴ The prefactor ξ_{ij} is nothing but the $\uparrow\uparrow$ -element of the product $\hat{U}^\dagger(\theta_i, \phi_i) \hat{U}(\theta_j, \phi_j)$:

$$\xi_{ij} = \cos \frac{\theta_i}{2} \cos \frac{\theta_j}{2} + \sin \frac{\theta_i}{2} \sin \frac{\theta_j}{2} e^{-(\phi_i - \phi_j)},$$

which satisfies the well known property: $\xi_{ij} = 1$ and 0 for the ferromagnetically and antiferromagnetically coupled spins, respectively. Therefore, in the DE limit, any antiferromagnetic (AFM) phase effectively breaks up into FM segments. For example, the description of the E -type AFM phase is reduced to the analysis of one-dimensional FM zigzag chains.^{4,19}

Next, we investigate abilities of the DE model for the description of the FE polarization. For these purposes, we calculate the electronic structure for the DE Hamiltonian [Eq. (7)], and then evaluate the electronic polarization, using the Berry-phase formula [the discrete analog of Eq. (3)].^{10,11} This procedure was applied to the series of orthorhombic manganites TbMnO_3 , HoMnO_3 , and YMnO_3 (and using both experimental and theoretically optimized crystal structure for the latter compound).^{7,8} The obtained polarization was compared with results of self-consistent HF calculations for the same low-energy model, but without additional approximations associated with the use of the DE limit. Typical results of such calculations are illustrated in Fig. 2 for the $Pbnm$ phase of YMnO_3 (other systems show very similar behavior). More specifically, we consider a twofold periodic magnetic texture, which is explained in Fig. 2(c), and keep the AFM coupling between adjacent planes $z = 0$ and $z = c/2$, as explained in Fig. 2(a). Then, $\phi = 0$ and 180° correspond to the AFM alignment of the E -type, while $\phi = 90^\circ$ corresponds to the spin-spiral alignment. For this geometry, the FE polarization should be parallel to the orthorhombic \mathbf{a} axis.⁵ In the DE model itself, we consider two levels of approximations. In the first case (denoted as ‘DE LDA’), we neglect $\hat{\mathcal{V}}_i^\dagger$ and consider only the crystal-field splitting and transfer integrals, derived from the LDA band structure. Then, the transfer integrals are modulated by ξ_{ij} ,

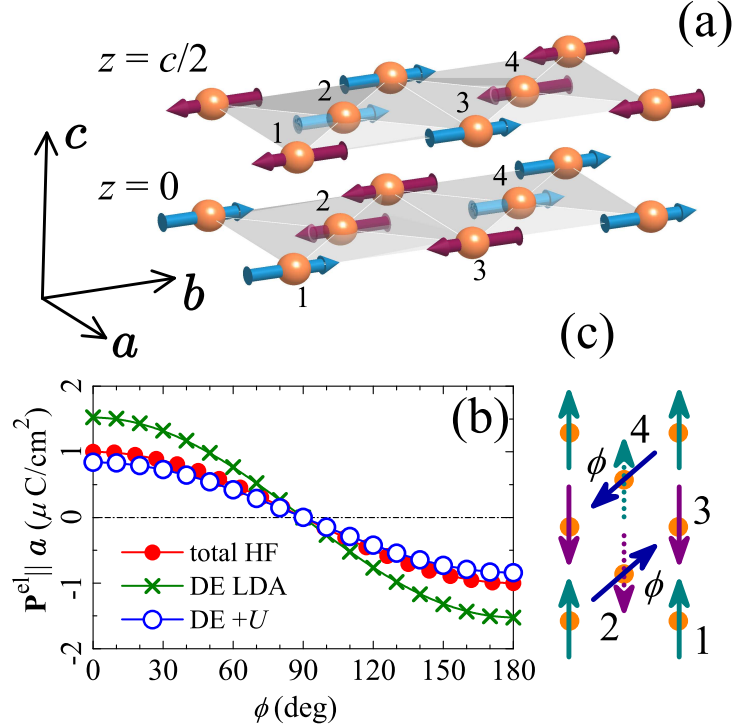


FIG. 2. (Color online) (a) *E*-type antiferromagnetic texture. (b) Behavior of electronic polarization in YMnO_3 upon rotation of magnetic moments as obtained in the self-consistent mean-field Hartree-Fock approximation (total HF); in the double exchange model for the LDA band structure (DE LDA); and in the double exchange model with the Hartree-Fock potential $\hat{\mathcal{V}}_i^\dagger$ (DE + U). In the rotated texture, the directions of spins at the sites 1 and 3 were fixed, while the spins at the sites 2 and 4 were rotated by the angle ϕ , as explained in panel (c). The planes $z = 0$ and $z = c/2$ were coupled antiferromagnetically.

as requested by the DE model. In the second case, we consider the full DE Hamiltonian, Eq. (7), including $\hat{\mathcal{V}}_i^\dagger$ (denoted as ‘DE + U ’). All magnetic solutions are insulating. Therefore, we can use the Berry-phase formula for the analysis of \mathbf{P}^{el} . The DE LDA scheme overestimates the electronic polarization by about 50 %. Nevertheless, this is to be expected, because LDA underestimates the band gap. Therefore, the FE polarization should be generally larger. Similar behavior was found in the first-principles calculations.^{5,17} The analytical expression, explaining the band-gap dependence of \mathbf{P}^{el} , will be derived in the next section. The band-gap problem is corrected by $\hat{\mathcal{V}}_i^\dagger$. Therefore, the FE polarization, derived in the DE + U scheme, is smaller. Moreover, results of self-consistent HF calculations for

the electronic polarization are well reproduced by the DE + U scheme: although \mathbf{P}^{el} in the approximate DE + U scheme is systematically smaller, the typical difference, which was obtained for all considered systems, is less than 15 %.

This is our main observation and also the main motivation of the rest of our work. By considering the DE limit, we will slightly lose in the accuracy. But instead we will be able to rationalize the problem and derive several analytical expressions for the FE polarization in orthorhombic manganites. Our analysis will also clarify results of the low-energy model and first-principles calculations.

III. RESULTS

We start with the analysis of the E -type AFM phase. As was pointed out above, in the DE limit, the FE AFM E -phase breaks up into one-dimensional FM zigzag chains. Therefore, the key moment for understanding the origin of the FE activity in the E -phase is the analysis of isolated zigzag chain.¹⁹ In Sec. III A, we start such an analysis with the simplest but analytically solvable model for the e_g electrons. In Sec. III B we will derive parameters of such a model, starting from a more general five-orbital model, which was obtained from the first-principles calculations.^{7,8,16} From the analysis of this model we will conclude that the situation, realized in most of the electronic structure calculations (even in ordinary LDA), corresponds to the limit of large energy splitting Δ between atomic e_g states, which incorporates the effects of the JT distortion and (optionally) the on-site Coulomb repulsion. Then, by considering the large- Δ limit, in Sec. III C we will derive an analytical expression for the FE polarization, which is based on the five-orbital model. This expression explains the functional dependence of \mathbf{P}^{el} on the relative directions of spins and the form of nearest-neighbor transfer integrals. In Sec. III D we will analyze relative directions of electronic and ionic polarizations in the noncentrosymmetric $P2_1nm$ structure and point out on the problem of structural optimization, which apparently exists in some of the first-principles calculations, where the directions of noncentrosymmetric atomic displacements are inconsistent with the type of the orbital ordering, realized in the FM zigzag chain. In Sec. III E, we discuss the possibility of switching the FE polarization by changing the magnetic texture: we argue that, even in the twofold periodic texture, there is another type of the AFM zigzag ordering, which leads to a finite FE polarization along the orthorhombic

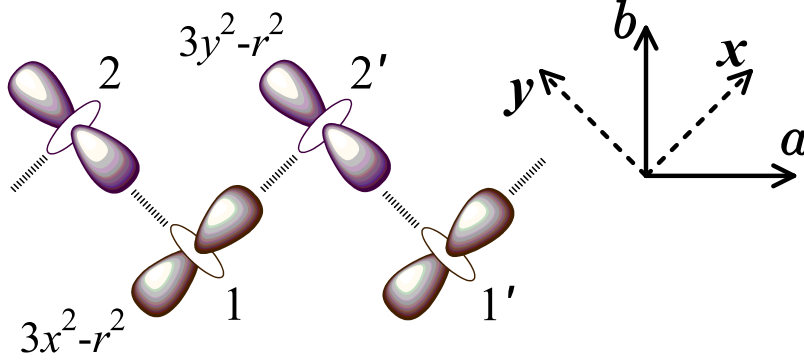


FIG. 3. (Color online) Geometry of the zigzag chain for the square lattice and the occupied e_g orbitals of the $3x^2-r^2$ and $3y^2-r^2$ type. Cubic and orthorhombic axes are denoted as \mathbf{xy} and \mathbf{ab} , respectively.

\mathbf{c} axis. However, the value of this polarization is expected to be small.

A. Analytically solvable model for the e_g electrons in the zigzag chain

The zigzag chain consists of the two groups of sites: the lower corner sites 1 and the upper corner sites 2 (see Fig. 3). The orthorhombic translation \mathbf{a} transforms each group to itself (the translated sites are denoted as $1'$ and $2'$, respectively). It is assumed that the lattice distortion stabilizes some e_g orbitals at the sites 1 and 2, which will be denoted as $|1\rangle_1$ and $|1\rangle_2$, respectively. The orthogonal to them e_g orbitals are denoted as $|2\rangle_1$ and $|2\rangle_2$, respectively. Furthermore, it is assumed that there is a symmetry operation (\hat{S}), which transforms the zigzag chain to itself and which consists of the 180° rotation around the \mathbf{a} axis (\hat{C}_a^2) with consequent translation. \hat{S} will transform site 1 to site 2, and vice versa. For the $Pbnm$ structure (and with some appropriate choice of the origin), such symmetry operation is $\{\hat{C}_a^2|\mathbf{a}/2+\mathbf{b}/2\}$ (where the first part stands for the rotation, and the second part specifies the translation) while for the $P2_1nm$ structure, it is $\{\hat{C}_a^2|\mathbf{a}/2+\mathbf{c}/2\}$. It is important that both symmetry operations include the translation $\mathbf{a}/2$. Then, it is convenient to work in the local basis, corresponding to the diagonal presentation of the e_g level splitting, such that \hat{S} would transform the basis functions of the site 1 to the ones of the site 2, and vice versa. Our idea is that, although we have two different sites, with such choice of the basis functions, the Hamiltonian becomes periodic with the period $\mathbf{a}/2$ and the problem can be

treated as if it would have only one site in the primitive cell. Similar idea was used for the analysis of the CE AFM state in the half-doped manganites.²⁰ Rather generally, these basis functions can be chosen in the form:

$$|1\rangle_1 = -\cos\beta|3z^2 - r^2\rangle_1 - \sin\beta|x^2 - y^2\rangle_1, \quad (8)$$

$$|2\rangle_1 = \sin\beta|3z^2 - r^2\rangle_1 - \cos\beta|x^2 - y^2\rangle_1 \quad (9)$$

at the site 1, and

$$|1\rangle_2 = -\cos\beta|3z^2 - r^2\rangle_2 + \sin\beta|x^2 - y^2\rangle_2, \quad (10)$$

$$|2\rangle_2 = \sin\beta|3z^2 - r^2\rangle_2 + \cos\beta|x^2 - y^2\rangle_2 \quad (11)$$

at the site 2, where $-\pi/2 < \beta \leq \pi/2$. $|\beta| = 60^\circ$ corresponds to the ideal square lattice, subjected to the JT distortion. Here, it is assumed that the direction of this distortion is determined by anharmonic electron-lattice interactions, which stabilize orbitals of the type $|1\rangle$ with $|\beta|$ close to 60° .^{13,21} Then, all deformations of the orbital ordering pattern are described by the single parameter β . Here, we continue to use the notations $|3z^2 - r^2\rangle$ and $|x^2 - y^2\rangle$ for the e_g orbitals, although it should be understood that they are valid only for the ideal square lattice, and more generally we have in mind some $|3z^2 - r^2\rangle$ -like orbitals, which transform to each other as $\hat{S}|3z^2 - r^2\rangle_1 = |3z^2 - r^2\rangle_2$, and some $|x^2 - y^2\rangle$ -like orbitals, which transform to each other as $\hat{S}|x^2 - y^2\rangle_1 = -|x^2 - y^2\rangle_2$. Such deformations of the ideal e_g orbitals can be caused, for example, by buckling distortions. It is easy to check that $\beta = -60^\circ$ yields $|1\rangle_1 = |3x^2 - r^2\rangle_1$, $|2\rangle_1 = |y^2 - z^2\rangle_1$, $|1\rangle_2 = |3y^2 - r^2\rangle_2$, and $|2\rangle_2 = |x^2 - z^2\rangle_1$; while $\beta = 60^\circ$ yields $|1\rangle_1 = |3y^2 - r^2\rangle_1$, $|2\rangle_1 = |z^2 - x^2\rangle_1$, $|1\rangle_2 = |3x^2 - r^2\rangle_2$, and $|2\rangle_2 = |z^2 - y^2\rangle_2$. Then, although in realistic situations, $|\beta|$ can deviate from 60° , we will say that $\beta < 0$ corresponds to the $3x^2 - r^2/3y^2 - r^2$ type of the orbital ordering (referring to the type of the occupied orbitals at the sites $1/2$), while $\beta > 0$ corresponds to the $3y^2 - r^2/3x^2 - r^2$ type of the orbital ordering.

As for the transfer integrals between e_g orbitals, we again consider a more general case and write them in the following form:

$$\hat{t}_{12'} = -\frac{1}{2} \left(\hat{\mathbb{I}} - |\sin\beta|\hat{\sigma}_x - \cos\beta\hat{\sigma}_z \right), \quad (12)$$

for the bond 1-2', and

$$\hat{t}_{12} = -\frac{1}{2} \left(\hat{\mathbb{I}} + |\sin\beta|\hat{\sigma}_x - \cos\beta\hat{\sigma}_z \right), \quad (13)$$

for the bond 1-2, in terms of the pseudospin Pauli matrices $\hat{\sigma}_x$, $\hat{\sigma}_y$, and $\hat{\sigma}_z$, and the 2×2 identity matrix $\hat{\mathbb{I}}$. Throughout this section, all energies are in the units of two-center integral t_0 of the $dd\sigma$ type.²² The form of \hat{t}_{ij} is suggested by the $dd\sigma$ transfer integrals in the ideal square lattice, which again corresponds to $\beta = 60^\circ$. Therefore, it is assumed that all deviations from the ideal square lattice are described by the single parameter β , similar to the orbital ordering. Note also that Eqs. (12) and (13) satisfy the idempotency condition $(\hat{t}_{ij})^2 = \hat{t}_{ij}$, which holds for the $dd\sigma$ transfer integrals in the square lattice.

Thus, in our model, the orbital ordering and the transfer integrals are described by the same parameter β . Generally speaking, these are different quantities, which should be specified by two different sets of parameters. Nevertheless, in the analytical model, one would always like to reduce the number of independent parameters to the minimum. Moreover, the use of the single parameter β is indeed a very reasonable approximation for our purposes:

- (i) At least for the ideal square lattice, the orbital ordering and the transfer integrals can be described by the same $|\beta| = 60^\circ$. Thus, there is the reference point where our construction is exact;
- (ii) Small deviations from the ideal case are treated as an approximation and we have some freedom to decide the form of this approximation. In Sec. IIIB we will show that typical deviations of $|\beta|$ from 60° are not large and, therefore, our approximation is robust;
- (iii) According to Eqs. (12) and (13), the transfer integrals do not depend on the sign of β (although the orbital ordering does). This is the very important requirement, because the phases of transfer integrals is determined solely by the geometry of the zigzag chain and should not depend on the type of the orbital ordering.

After the transformation to the local basis, given by Eqs. (8)-(11), the transfer integrals become:

$$\hat{\mathbf{t}}_{12'} = \hat{\mathbf{t}}_{21} = \frac{1}{2} \left(\cos \beta \hat{\mathbb{I}} + \sin 2\beta \hat{\sigma}_x - i |\sin \beta| \hat{\sigma}_y - \cos 2\beta \hat{\sigma}_z \right), \quad (14)$$

where $\hat{\mathbf{t}}_{2'1} = \hat{\mathbf{t}}_{12} = \hat{\mathbf{t}}_{21}^T$. Thus, the transfer integrals are indeed periodic with the period $\mathbf{a}/2$ and, in the reciprocal space, the problem is reduced to the analysis of the 2×2 Hamiltonian of the form:

$$\hat{\mathcal{H}}(k) = \varepsilon(k) + \mathbf{d}(k) \cdot \hat{\boldsymbol{\sigma}},$$

where $\varepsilon(k) = \cos \beta \cos(ka/2)$, and components of the vector $\mathbf{d} \equiv (d_x, d_y, d_z)$ are given by $d_x = \sin 2\beta \cos(ka/2)$, $d_y = |\sin \beta| \sin(ka/2)$, and $d_z = -\cos 2\beta \cos(ka/2) - \Delta/2$. The parameter Δ in d_z is the intra-atomic energy splitting between e_g states, caused by lattice distortions and Coulomb interactions. This result can be also viewed as if the transformation (8)-(11) would “straightened” the zigzag chain and made it equivalent to a linear chain, but with different transfer integrals operating in the positive and negative directions of \mathbf{a} . Because of the condition $\hat{\mathbf{t}}_{12} = \hat{\mathbf{t}}_{21}^T$, the transfer integrals are generally not centrosymmetric with respect to the atomic sites and the system will develop a finite electronic polarization. Nevertheless, in the limit $\Delta \rightarrow \infty$, the basis orbitals of the type ‘2’ are projected out. Then, the transfer integrals between orbitals of the same type ‘1’ are just scalars, and the condition $\hat{\mathbf{t}}_{12} = \hat{\mathbf{t}}_{21}^T$ becomes equivalent to $\mathbf{t}_{12} = \mathbf{t}_{21}$. Thus, in the limit $\Delta \rightarrow \infty$, the problem should become centrosymmetric. From this point of view, it is logical to consider the limit $\Delta \rightarrow \infty$ as the reference point for the electronic polarization.

The eigenvalues of $\hat{\mathcal{H}}(k)$ are given by $E_{\pm}(k) = \varepsilon(k) \pm |\mathbf{d}(k)|$, and the eigenvector, corresponding to the lowest occupied band, satisfies the condition: $[\mathbf{d}(k) \cdot \hat{\boldsymbol{\sigma}} + |\mathbf{d}(k)|]|-, k\rangle = 0$.²³ Then, $|-, k\rangle$ can be taken in the form:

$$|-, k\rangle = \begin{pmatrix} C_1(k) \\ e^{i\gamma(k)} C_2(k) \end{pmatrix},$$

where

$$C_1(k) = \frac{1}{\sqrt{2}} \left(1 - \frac{d_z(k)}{|\mathbf{d}(k)|} \right)^{1/2},$$

$$C_2(k) = -\frac{1}{\sqrt{2}} \left(1 + \frac{d_z(k)}{|\mathbf{d}(k)|} \right)^{1/2},$$

and $\gamma(k) = \arctan(d_y/d_x)$.

At the half-filling (one e_g electron per each Mn site), the zigzag chain is a band insulator. This property holds even for $\Delta = 0$ due to specific form of the $dd\sigma$ transfer integrals.²⁴ Moreover, the reciprocal lattice vector of the “straightened” chain is $G = 4\pi/a$, and $|-, k\rangle$ is a periodic function of G . Therefore, the electronic polarization can be computed directly, using the formula of King-Smith and Vanderbilt.¹⁰ Note that in this section, it is more convenient to work with the electric dipole moment, rather than with the polarization density. Therefore, Eq. (3) was additionally multiplied by the primitive cell volume V . Nevertheless, unless it is specified otherwise, we will use the same notations for this quantity and

continue to call it “the polarization”. Then, we obtain the following expression for the FE polarization parallel to the orthorhombic \mathbf{a} axis (per two Mn sites in the zigzag chain):

$$P_E^{\text{el}} = \frac{ea}{2\pi} \int_{-2\pi/a}^{2\pi/a} C_2^2(k) \frac{d\gamma(k)}{dk} dk,$$

which can be further transformed to

$$P_E^{\text{el}} = \frac{ea^2}{4\pi} \int_0^{2\pi/a} \frac{|\sin \beta| \sin 2\beta}{|\mathbf{d}(k)| [|\mathbf{d}(k)| - d_z(k)]} dk, \quad (15)$$

where the subscript E means that this polarization corresponds to the E -type AFM phase in the DE limit.

Thus, we immediately recognize that when the orbital ordering changes from $3x^2-r^2/3y^2-r^2$ ($\beta < 0$) to $3y^2-r^2/3x^2-r^2$ ($\beta > 0$), the polarization changes its sign.

Then, it is straightforward to find that

$$\lim_{\Delta \rightarrow 0^+} P_E^{\text{el}} = \frac{|\sin \beta|}{\sin \beta} \frac{ea}{2}$$

and, therefore, $|P_E^{\text{el}}| = ea/2$ (see Ref. 25). Then, since P_E^{el} is well defined modulo ea ,¹⁰ the values of P_E^{el} and $-P_E^{\text{el}}$ for $\Delta = 0$ are equivalent. Such a situation means that the system possesses the inversion symmetry, but the inversion centers are located in the middles of the bonds.²⁶ Thus, by removing the JT distortion from our model, we effectively create a new inversion center. This is indeed the case for the model considered above: since $\hat{t}_{12} = \hat{t}_{21}$ and $\hat{t}_{12'} = \hat{t}_{2'1}$ [see Eqs. (12)-(13)], the transfer integrals are centrosymmetric with respects to the middles of the bonds.

In the limit $\Delta \rightarrow \infty$, we have

$$P_E^{\text{el}}(\Delta \rightarrow \infty) \rightarrow \frac{ea |\sin \beta| \sin 2\beta}{\Delta^2}. \quad (16)$$

This result also has a transparent physical meaning and can be easily understood by starting from the expression

$$P_E^{\text{el}} = -2e \int x w^2(x) dx, \quad (17)$$

in terms of the Wannier functions,¹⁰ where the prefactor ‘2’ stands for the number of Mn sites in the primitive cell of the zigzag chain. Let us consider the limit $\Delta \rightarrow \infty$, where $|w_\infty\rangle = |1\rangle_1$ and it is centered at the site 1 (see Fig. 3). Then, in the first order of $1/\Delta$, this Wannier function will have a finite tail, spreading to the neighboring sites 2 and 2’, which

are located at $x = -a/2$ and $a/2$, respectively. In the first order of perturbation theory, this tail is proportional to the transfer integrals [Eq. (14)] from the occupied orbital $|1\rangle_1$ to the subspace of unoccupied orbitals $|2\rangle$ at the sites 2 and 2'. Then, by assuming that all weights of $w^2(x)$ are accumulated at the lattice points (that is the meaning of the “lattice model”), one can write that

$$w^2(x) = (1 - q_- - q_+)\delta(x) + q_-\delta(x + a/2) + q_+\delta(x - a/2),$$

where

$$q_{\pm} = \left(\frac{\sin 2\beta \mp |\sin \beta|}{2\Delta} \right)^2$$

are the weights of $w^2(x)$ at the sites 2 and 2'. By substituting this $w^2(x)$ into Eq. (17), we again arrive at Eq. (16). Thus, in terms of these arguments, the polarization is finite because $q_+ \neq q_-$. Alternatively, one can say that due to the asymmetric electron transfer, the Wannier centers are shifted from the centrosymmetric atomic positions.¹⁸ For a given Δ , the difference $(q_+ - q_-)$ depends on the value of β and takes the maximal value when $|\beta| = |\beta_{\max}| = \arctan \sqrt{2}$ (about 54.7°).

The behavior of electronic polarization as the function of intra-atomic energy splitting between e_g states is summarized in Fig. 4.

A very similar model of the FE polarization in orthorhombic manganites was considered by Barone *et al.*¹⁹ The advantage of our approach is that we were able to reduce the problem to the 2×2 Hamiltonian in the reciprocal space and to solve it analytically. Such an analysis provides a transparent physical picture for the behavior of the FE polarization. Therefore, we would like to stress briefly the difference between our results and the ones by Barone *et al.* First, the behavior of polarization, obtained by Barone *et al.*, is very different from ours: it is zero for $\Delta = 0$ and approaches $\pm ea/2$ for $\Delta \rightarrow \infty$. Nevertheless, such a difference can be easily understood by the different choice of the reference point in the calculations of P_E^{el} : $\Delta \rightarrow \infty$ in our work and $\Delta = 0$ in the work of Barone *et al.* Another discrepancy is related to the functional dependence of the orbital ordering and the FE polarization on Δ : in the work of Barone *et al.*, these two quantities become finite starting only from some critical value of Δ . We believe that such a behavior is counterintuitive (at least, in the framework of the considered model) and the orbital ordering, as well as the FE polarization, should evolve continuously starting from $\Delta = 0$ (see also the analysis of the orbital ordering for similar model, reported in Ref. 24).

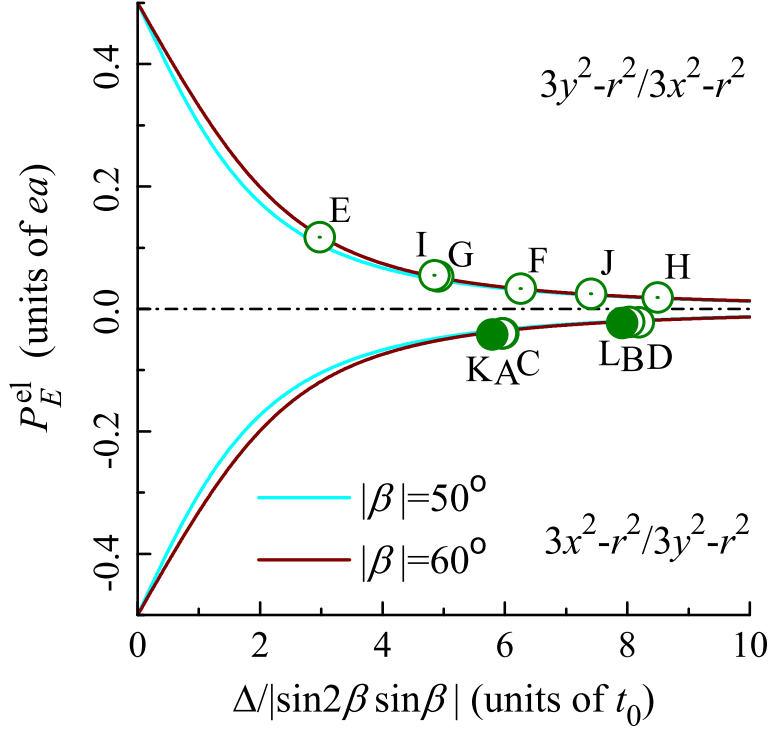


FIG. 4. (Color online) Electronic polarization (more precisely – the electric dipole moment) for the isolated zigzag chain as the function of intra-atomic energy splitting between e_g states. Upper part corresponds to the $3y^2-r^2/3x^2-r^2$ type of the orbital ordering ($\beta>0$) and lower part corresponds to the $3x^2-r^2/3y^2-r^2$ type of the orbital ordering ($\beta<0$). The values obtained for YMnO_3 are shown by open symbols. The points A, C, E, G, I denote the bare LDA values, obtained for the experimental $P2_1nm$ and $Pbnm$ structures, and three theoretical structures, obtained in LSDA and LDA+ U with $U=2.2$ and 6.0 eV, respectively. Similar values, obtained after adding the HF potentials, are denoted as B, D, G, H, and J, respectively. The values obtained for the experimental $Pbnm$ structure of HoMnO_3 are shown by filled symbols: the point K denotes the bare LDA value and the point L takes into account the effect of the HF potential.

B. Parameters of the e_g model and values of electronic polarization for YMnO_3 and HoMnO_3

In this section, we evaluate parameters of the e_g model for realistic compounds, such as YMnO_3 and HoMnO_3 . For these purposes, we do the following:

- (i) We start with the realistic low-energy model, derived for the Mn $3d$ bands of YMnO_3

and HoMnO_3 on the basis of first-principles electronic structure calculations (results of Refs. 16 and 8);

- (ii) Then, we pick up parameters of the model for the single zigzag chain, propagating along the orthorhombic \mathbf{a} axis (and assuming that, in the DE limit, all transfer integrals in the directions \mathbf{b} and \mathbf{c} are blocked by the E -type AFM ordering);
- (iii) Solve the electronic structure problem for the isolated zigzag chain; find eigenvalues and eigenfunctions;
- (iv) Construct the Wannier functions for the upper lying e_g bands. For these purposes, we use the projector-operator technique and trial orbitals, obtained from the diagonalization of the site-diagonal part of the density matrix;¹⁵
- (v) Find parameters of the e_g model in the obtained Wannier basis;
- (vi) Transform the parameters to the crystal-field representation, which diagonalizes the site-diagonal part of the e_g model;
- (vii) Fit the transfer integrals for the bond 1-2' in terms of t_0 and β , by using the functional dependence given by Eq. (14). Meanwhile, the splitting Δ between the e_g states is obtained from the site-diagonal part.

For YMnO_3 , we have considered several crystal structures, which were previously discussed in Ref. 8:

- (i) The experimental $Pbnm$ and $P2_1nm$ structures, reported in Ref. 17;
- (ii) Three theoretical $P2_1nm$ structures, which were optimized in the local-spin-density approximation (LSDA) and LDA+ U with $U = 2.2$ and 6.0 eV by assuming the collinear E -type AFM alignment without SO interaction. The results of this optimization can be found in Ref. 8.

For HoMnO_3 , we use the experimental $Pbnm$ structure, reported in Ref. 27.

Parameters of the e_g model, obtained from the fitting, are summarized in Table I. Eq. (14) captures main details of transfer integrals between the nearest neighbors. The largest deviation from the ideal $|\beta| = 60^\circ$ case was found if one uses the bare LDA parameters, derived

TABLE I. Parameters of the e_g model for the isolated zigzag chain, derived for HoMnO_3 (HMO) and different structures of YMnO_3 (YMO): the experimental $Pbnm$ and $P2_1nm$ structures, reported in Ref. 17, and three $P2_1nm$ structures, which were theoretically optimized in LSDA and LDA+ U with $U=2.2$ and 6.0 eV by assuming the collinear E -type AFM alignment (results of Ref. 8). In this Table, t_0 is the effective two-center integral $dd\sigma$, Δ is the intra-atomic splitting between e_g states, and β specifies the form of the transfer integrals in the Mn-Mn bonds. The values, obtained by using bare LDA parameters are denoted as ‘LDA’, and the ones after adding the Hartree-Fock potential are denoted as ‘+ U ’.

	t_0 (meV)		Δ (eV)		β (degrees)	
	LDA	+ U	LDA	+ U	LDA	+ U
HMO ($Pbnm$, Exp.)	341	353	1.52	2.15	-54.0	-55.3
YMO ($Pbnm$, Exp.)	335	348	1.53	2.18	-54.2	-55.8
YMO ($P2_1nm$, Exp.)	334	346	1.54	2.15	-54.1	-55.7
YMO ($P2_1nm$, LSDA)	405	412	0.92	1.95	57.6	59.1
YMO ($P2_1nm$, $U=2.2$ eV)	361	370	1.37	2.41	55.1	57.3
YMO ($P2_1nm$, $U=6.0$ eV)	348	359	1.30	2.04	54.4	56.1

for the experimental $Pbnm$ structure of HoMnO_3 . In this case, the agreement between the original matrices $\hat{t}_{12'}$ and results of the fitting using Eq. (14) is the worst:

$$\hat{t}_{12'} = \begin{pmatrix} 119 & -328 \\ -12 & 39 \end{pmatrix} \quad \text{and} \quad \begin{pmatrix} 153 & -300 \\ -24 & 47 \end{pmatrix},$$

before and after the fitting, respectively, in units of meV. On the other hand, β becomes close to 60° if one uses theoretical LSDA crystal structure of YMnO_3 and takes into account the additional level splitting, caused by the HF potential. In this case, the agreement between the original and fitted matrices is nearly perfect. Nevertheless, we would like to emphasize that the analytical expression, given by Eq. (15), with the parameters, derived from the fitting, excellently reproduces the behavior of electronic polarization, obtained in the same e_g model but without fitting (see Fig. 5). Thus, deviations of transfer integrals from Eq. (14) are relatively unimportant for the analysis of the FE polarization.

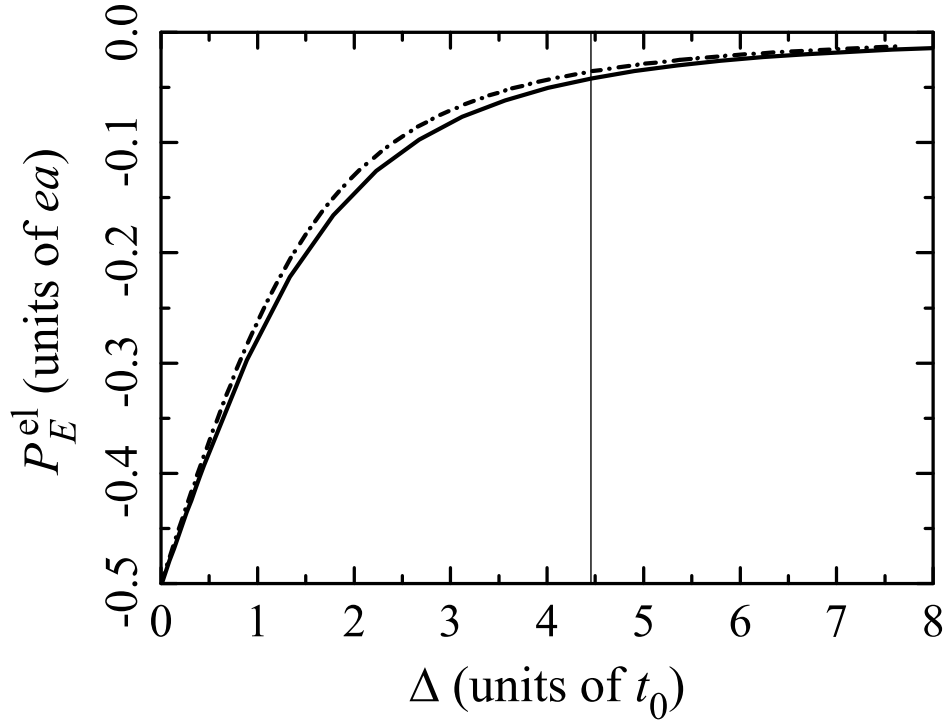


FIG. 5. Electronic polarization (more precisely – the electric dipole moment) in the e_g model for the isolated zigzag chain as obtained by using bare LDA parameters for HoMnO_3 (solid line) and after the parametrization of transfer integrals using Eq. (14). The vertical line shows the bare LDA value of Δ/t_0 . The parameters are taken from Table I.

It is interesting to note that $|P_E^{\text{el}}| = ea/2$ when $\Delta \rightarrow 0^+$ (see Fig. 5). This means that in the limit $\Delta \rightarrow 0$, the system behaves such as if it would be centrosymmetric with respect to the bond centers,²⁶ even despite the fact that the space groups $Pbnm$ and $P2_1nm$ (so as the transfer integrals) do not have such symmetry. Apparently, such a behavior is related to a more general symmetry of the transfer integrals.

Then, we take the values of FE polarization, obtained for the e_g band (without fitting) and also plot them on Fig. 4. As for the abscissa coordinates, we use results of Table I. We can clearly see that all these values fall on the analytical dependence, derived for the e_g model. The main parameter, which controls the value of the FE polarization, is the ratio Δ/t_0 . The β -dependence of P_E^{el} is less important. This result is very natural and will be discussed in a moment. Moreover, the physically relevant situation, realized in the orthorhombic manganites, always corresponds to the limit of large Δ . This is another important finding,

which will allow us to further rationalize the behavior of the FE polarization in Sec. III C.

The polarization has different sign for the experimental and theoretical structures, that indicates at different types of the orbital ordering in the zigzag chain. In the $Pbnm$ phase, all zigzag chains are equivalent, and in Fig. 4 we simply picked up the one with the same orbital ordering as in the $P2_1nm$ phase. However, in the $P2_1nm$ phase, the type of the zigzag chain is uniquely defined (as the one with larger Mn-Mn distances, which stabilize the FM coupling in the zigzag chain). Therefore, the sign difference between experimental and theoretical values of P_E^{el} in the $P2_1nm$ phase indicates at a serious problem, which may exist in the first-principles calculations. The problem will be discussed in details in Sec. III D.

Then, all values of $|\beta|$ are close to $|\beta_{\text{max}}| \approx 54.7^\circ$, which corresponds to the maximum of $|P_E^{\text{el}}|$ (see Table I). Therefore, any deviation of $P_E^{\text{el}}(\beta)$ from $P_E^{\text{el}}(\beta_{\text{max}})$ will be only of the order of $(\beta - \beta_{\text{max}})^2$. Thus, all the effects of β on P_E^{el} will be small. This can be clearly seen in Fig. 6, where we plot P_E^{el} versus Δ/t_0 , using different sets of parameters for the e_g model and varying Δ : all lines, corresponding to different crystal structures and different levels of approximation for the on-site interactions (with and without the HF potential), are practically undistinguishable. This means that, in reality, P_E^{el} is controlled by only two sets of parameters: (i) the ratio Δ/t_0 , and (ii) the lattice parameters a , b , and c , which determine the value of the scaling factor a/V in the polarization density. The β -dependence of P_E^{el} is relatively unimportant.

From the physical point of view, the β -dependence of the transfer integrals is related to the buckling of the Mn-O-Mn bonds. Then, the above result suggests that P_E^{el} does not explicitly depend on the Mn-O-Mn angles: the latter can contribute to P_E^{el} , but only via other model parameters (such as t_0), which depend on these angles. This finding is consistent with the conclusion of Ref. 18, based on the first-principles electronic structure calculations.

Finally, we briefly explain the correspondence between the values of the electric dipole moment in Fig. 4 and the polarization density. Let us consider the experimental $Pbnm$ structure of YMnO_3 . Then, the value $-0.022ea$, which takes into account the effect of the HF potential, corresponds to the polarization density of about $-1.65 \mu\text{C}/\text{cm}^2$. It should be remembered that it is only the contribution of the e_g band alone. In order to obtain the total polarization for the five-orbital model, it should be combined with the contribution of the t_{2g} band. This yields the total polarization $-0.84 \mu\text{C}/\text{cm}^2$, which agrees with the

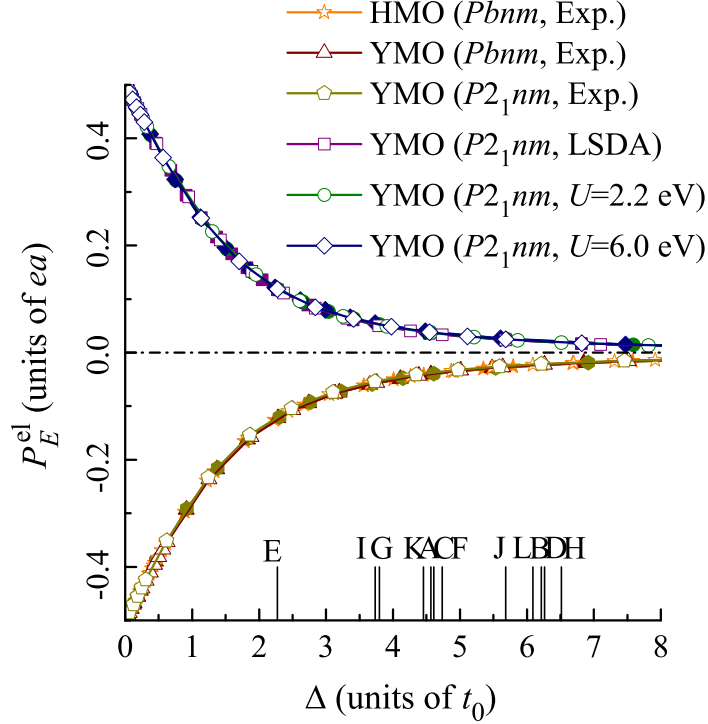


FIG. 6. (Color online) Electronic polarization (more precisely – the electric dipole moment) versus Δ/t_0 , as obtained using various sets of parameters for the e_g model. Results of bare LDA and after including the Hartree-Fock potential are shown by filled and open symbols, respectively. The positions of Δ/t_0 for different systems are shown by capital letters. The points A, C, E, G, I stand for the bare LDA values of Δ/t_0 , corresponding to the experimental $P2_1nm$ and $Pbnm$ structures, and three theoretical structures, obtained in LSDA and LDA+ U with $U=2.2$ and 6.0 eV, respectively. Similar points, obtained after adding the Hartree-Fock potential, are denoted as B, D, G, H, and J, respectively. The points K and L correspond to the $Pbnm$ structure of HoMnO_3 , obtained in the bare LDA and after including the HF potential, respectively.

value for the E -type AFM state (for $\phi = 180^\circ$) in Fig. 2. Thus, the contributions of the t_{2g} and e_g bands have opposite sign and partially cancel each other, in agreement with the first-principles calculations.¹⁸ In the rest of this work, we will deal with the total polarization density, including the effect of both t_{2g} and e_g bands.

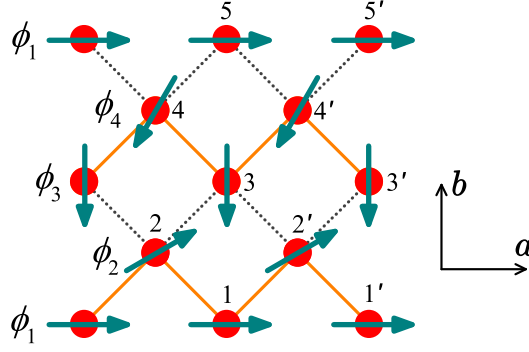


FIG. 7. (Color online) General twofold periodic magnetic texture in the \mathbf{ab} plane of orthorhombic manganites, which remains invariant under the symmetry operation $\hat{S} = \{\hat{C}_a^2 | \mathbf{a}/2 + \mathbf{b}/2\}$ of the space group $Pbnm$. Solid and dotted lines denote two types of magnetically inequivalent bonds.

C. Electronic polarization in the five-orbital model: simple analytical expression

Now, we will generalize results of two previous sections and derive an approximate, but very transparent expression for the electronic polarization in orthorhombic manganites with a general twofold periodic magnetic texture. Our starting point is that the behavior of electronic polarization in realistic compounds corresponds to the limit of large Δ . This limit can be justified even without on-site Coulomb interactions (i.e., considering the ratio of transfer integrals to the crystal-field splitting in bare LDA), and is additionally strengthened after including the Coulomb interactions. Thus, the central quantity, which we should evaluate in the second order of $1/\Delta$, is the weight $w_{i \rightarrow j}^2$, transferred from the Wannier orbital at the site i to the neighboring site j . Moreover, since electronic polarization is equal to zero for the fully occupied band, it is more convenient to start with the unoccupied e_g orbitals and consider the transfer integrals to the subspace of three t_{2g} and one e_g occupied orbitals at each of the neighboring sites. This procedure should give us $-\mathbf{P}^{\text{el}}$.

The transfer integrals obey certain symmetry rules and, in the DE model, are additionally modulated by ξ_{ij} . More specifically, we consider a planar magnetic texture which is shown in Fig. 7. The periodicity of this texture along the orthorhombic axes is a and $2b$, respectively. The directions of spins are specified by three azimuthal angles: ϕ_2 , ϕ_3 , and ϕ_4 (while $\phi_1 = 0$ is treated as the reference point). Moreover, we assume that the DE Hamiltonian remains invariant under the symmetry operation $\hat{S} = \{\hat{C}_a^2 | \mathbf{a}/2 + \mathbf{b}/2\}$, which transforms the bond 1-2

to 4'-3, the bond 3-2 to 4-5, etc. In the DE model, it imposes additional conditions on the azimuthal angles: $\cos \frac{\phi_2}{2} = \cos \frac{\phi_3 - \phi_4}{2}$ and $\cos \frac{\phi_4}{2} = \cos \frac{\phi_3 - \phi_2}{2}$, which are satisfied if $\phi_3 = \phi_2 \pm \phi_4$ (modulo 2π). Thus, the magnetic texture is specified by only two independent parameters ϕ_2 and ϕ_4 , similar to the magnetic texture obtained in the mean-field HF calculations with the SO coupling.^{7,8}

Then, we consider some central site (say, site 3 in Fig. 7) and evaluate its contribution to the electronic polarization, which is caused by the Wannier weight transfer to the neighboring sites 4', 4, 2, and 2', located at $(\mathbf{a} + \mathbf{b})/2$, $-(\mathbf{a} - \mathbf{b})/2$, $-(\mathbf{a} + \mathbf{b})/2$, and $-(\mathbf{a} - \mathbf{b})/2$, respectively. In the second order of $1/\Delta$ (and apart from the proportionality coefficient, which will be specified later), the contribution of the site 3 to the vector of electronic polarization can be written as

$$\mathbf{P}_3^{\text{el}} \sim \frac{e}{2} \cos^2 \frac{\phi_2}{2} [(\mathbf{a} + \mathbf{b})w_{3 \rightarrow 4'}^2 - (\mathbf{a} - \mathbf{b})w_{3 \rightarrow 4}^2] + \frac{e}{2} \cos^2 \frac{\phi_4}{2} [(\mathbf{a} - \mathbf{b})w_{3 \rightarrow 2'}^2 - (\mathbf{a} + \mathbf{b})w_{3 \rightarrow 2}^2], \quad (18)$$

where $w_{i \rightarrow j}^2$ is proportional to the sum of squares of the transfer integrals from the unoccupied orbital 5 at the site i to the occupied orbitals 1-4 at the site j : $w_{i \rightarrow j}^2 = [(\mathbf{t}_{ij}^{51})^2 + (\mathbf{t}_{ij}^{52})^2 + (\mathbf{t}_{ij}^{53})^2 + (\mathbf{t}_{ij}^{54})^2] / \Delta^2$. These transfer integrals should be calculated in the 'crystal-field representation', that diagonalizes the site-diagonal part of the one-electron Hamiltonian. The parameter Δ is understood as the energy difference between the unoccupied orbital 5 and the center of gravity of occupied orbitals 1-4 (see Fig. 8). Thus, in this analysis, we neglect the splitting between the occupied orbitals, which is smaller than Δ . Then, in the $Pbnm$ structure, each Mn site is located in the inversion center. Therefore, $w_{i \rightarrow j}^2$ in the bonds 3-4' and 3-2 (as well as 3-2' and 3-4) are equivalent, and Eq. (18) can be further transformed to

$$\mathbf{P}_3^{\text{el}} \sim \frac{e}{4} (\cos \phi_2 - \cos \phi_4) [(\mathbf{a} + \mathbf{b})w_{3 \rightarrow 4'}^2 - (\mathbf{a} - \mathbf{b})w_{3 \rightarrow 4}^2]. \quad (19)$$

Similar analysis can be performed for another Mn site in the primitive cell (say, site 4' in Fig. 7). Moreover, since the sites 3 and 4' are connected by the symmetry operation $\hat{S} = \{\hat{C}_a^2 | \mathbf{a}/2 + \mathbf{b}/2\}$, using Eq. (19), one can immediately obtain that

$$\mathbf{P}_{4'}^{\text{el}} \sim \frac{e}{4} (\cos \phi_2 - \cos \phi_4) [(\mathbf{a} - \mathbf{b})w_{3 \rightarrow 4'}^2 - (\mathbf{a} + \mathbf{b})w_{3 \rightarrow 4}^2].$$

Then, the total polarization $\mathbf{P}^{\text{el}} = 2(\mathbf{P}_3^{\text{el}} + \mathbf{P}_{4'}^{\text{el}})$ can be evaluated as

$$\mathbf{P}^{\text{el}} = \frac{e}{V} (\cos \phi_2 - \cos \phi_4) [w_{3 \rightarrow 4'}^2 - w_{3 \rightarrow 4}^2] \mathbf{a}.$$

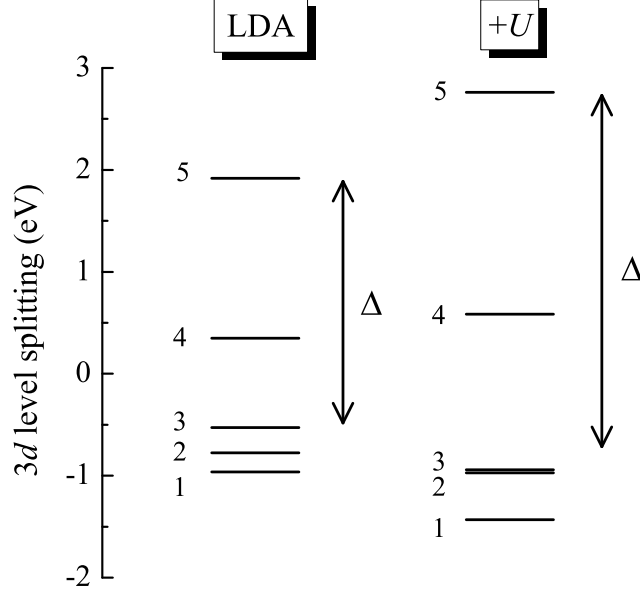


FIG. 8. Splitting of $3d$ levels for the experimental $Pbnm$ phase of $YMnO_3$. The values, obtained using bare LDA parameters of the low-energy model are denoted as ‘LDA’, and the ones obtained after adding the Hartree-Fock potential are denoted as ‘+U’. Δ is the energy splitting between the unoccupied orbital 5 and the center of gravity of occupied orbitals 1-4.

Here, V is the primitive cell volume, containing four Mn sites (two in each of the \mathbf{ab} planes, located at $z=0$ and $c/2$, which is reflected in the additional prefactor 2 in the above expression). Finally, by applying the symmetry operation $\hat{S} = \{\hat{C}_a^2 | \mathbf{a}/2 + \mathbf{b}/2\}$, the sites 3 and 4 can be transformed to the sites 4’ and 3, respectively. Thus, \mathbf{P}^{el} can be expressed through the transfer integrals in only one nearest-neighbor (NN) bond 3-4’ (or in any equivalent to it bond):

$$\mathbf{P}^{\text{el}} = \frac{1}{2} (\cos \phi_2 - \cos \phi_4) \mathbf{P}_E^{\text{el}}, \quad (20)$$

where

$$\mathbf{P}_E^{\text{el}} = \frac{2e}{V} [w_{3 \rightarrow 4'}^2 - w_{4' \rightarrow 3}^2] \mathbf{a} \quad (21)$$

is the electronic polarization in the E -type AFM state. For an arbitrary direction of spin at the site 1, the angular dependence $(\cos \phi_2 - \cos \phi_4)$ in Eq. (20) should be replaced by a more general expressions $\mathbf{e}_1 \cdot (\mathbf{e}_2 - \mathbf{e}_4)$. Eqs. (20) and (21) allow us to rationalize many aspects of the multiferroic activity in manganites with the twofold periodic magnetic texture, namely:

- (i) \mathbf{P}^{el} is parallel to the orthorhombic \mathbf{a} axis;

- (ii) If $\phi_4 = \phi_2 + \pi$, \mathbf{P}^{el} is proportional to $\cos \phi_2$, which nicely explains the functional dependence of $\mathbf{P}^{\text{el}}(\phi)$ in Fig. 2(b) and in the first-principles calculations for the same magnetic geometry (Ref. 5);
- (iii) \mathbf{P}^{el} vanishes in the homogeneous spin-spiral state ($\phi_2 = \pi/2$ and $\phi_4 = 3\pi/2$). This is a very natural result from the viewpoint of the DE physics: in the spin-spiral texture, all $|\xi_{ij}|$ are the same. Therefore, all bonds remain equivalent, and the inversion symmetry of the DE Hamiltonian is not broken;
- (iv) Since $\hat{\mathbf{t}}_{ji} = \hat{\mathbf{t}}_{ij}^T$, \mathbf{P}_E^{el} can be also presented in the form

$$\mathbf{P}_E^{\text{el}} = \frac{2e}{V} \frac{(\vec{v}_+, \vec{v}_-)}{\Delta^2} \mathbf{a}, \quad (22)$$

where (\vec{v}_+, \vec{v}_-) is the scalar product of the 4-dimensional vectors $\vec{v}_{\pm} \equiv (v_{\pm}^1, v_{\pm}^2, v_{\pm}^3, v_{\pm}^4)$, constructed from symmetric (+) and antisymmetric (−) parts of the transfer integrals: $v_{\pm}^m = \mathbf{t}_{ij}^{5m} \pm \mathbf{t}_{ij}^{m5}$. Thus, in order to have finite \mathbf{P}^{el} , the matrix of transfer integrals should have both symmetric and antisymmetric components.

Let us evaluate $\mathbf{P}_E^{\text{el}} \equiv (P_E^{\text{el}}, 0, 0)$, using Eq. (22), for the experimental *Pbnm* phase of YMnO₃. In this case, the unit cell volume is $V = 224.13 \text{ \AA}^3$ and the orthorhombic lattice parameter is $a = 5.245 \text{ \AA}$.¹⁷ Then, for the bare LDA band structure, we have: $\Delta = 2.40 \text{ eV}$ (see Fig. 8), $\vec{v}_+ = (-125, 18, 15, 336) \text{ meV}$, and $\vec{v}_- = (99, -49, -25, -314) \text{ meV}$ (all parameters of the low-energy model for YMnO₃ can be found in Supplemental Material of Ref. 8). By substituting all these values in Eq. (22), we obtain $P_E^{\text{el}} = -1.55 \text{ } \mu\text{C}/\text{cm}^2$, which agrees very well with the value of $-1.53 \text{ } \mu\text{C}/\text{cm}^2$, obtained directly from the Berry-phase formula [Eq. (3)], without additional approximations (apart from the DE limit). For the more realistic case, including the effect of the HF potential, we have: $\Delta = 3.45 \text{ eV}$, $\vec{v}_+ = (6, -117, 26, 335) \text{ meV}$, and $\vec{v}_- = (10, 91, -24, -319) \text{ meV}$. Then, Eq. (22) yields $P_E^{\text{el}} = -0.74 \text{ } \mu\text{C}/\text{cm}^2$, which is again consistent with the value of $-0.85 \text{ } \mu\text{C}/\text{cm}^2$, obtained directly from the Berry phase formula [Eq. (3)]. Moreover, the values of the scalar product (\vec{v}_+, \vec{v}_-) appear to be very close when they are calculated with and without the HF potential: -0.118 and -0.119 eV^2 , respectively. This result is very natural because the form of the crystal-field orbitals in orthorhombic manganites is mainly controlled by the JT distortion: the latter is large and thus ‘decides’ which orbitals will be occupied and which will not. On the other hand, the effect of on-site Coulomb interactions, being inversely proportional to

U ,¹³ is considerably smaller. Thus, although the Coulomb interactions contribute to the splitting between occupied and empty states (see Fig. 8), they practically do not change the subspace of occupied orbitals. Therefore, the construction (\vec{v}_+, \vec{v}_-) , which is evaluated in the crystal-field representation, will not strongly depend on whether it is calculated with or without the HF potential. In such a situation, the absolute value of P_E^{el} will be mainly controlled by the parameter Δ in the denominator of Eq. (22).

Furthermore, Δ can be presented in the form: $\Delta = \Delta_{\text{JT}} + \Delta_U$, where Δ_{JT} and Δ_U take into account the effects of the bare JT distortion and the on-site Coulomb interactions, respectively. In the example considered above, Δ_{JT} is the LDA level splitting and Δ_U is the additional splitting, caused by the HF potential (see Fig. 8). Then, if $P_E^{\text{el}}(0)$ is the FE polarization in LDA, the effect of on-site Coulomb interactions on P_E^{el} can be evaluated using the following scaling relation:

$$P_E^{\text{el}}(\Delta_U) = P_E^{\text{el}}(0)/(1 + \Delta_U/\Delta_{\text{JT}})^2,$$

which was observed in many LDA+ U calculations, treating the on-site Coulomb repulsion U as an adjustable parameter.^{5,17}

Finally, it is instructive to evaluate $\mathbf{P}^{\text{el}} \equiv (P^{\text{el}}, 0, 0)$ for the noncollinear magnetic ground state of YMnO₃ using Eq. (20). This magnetic ground state was obtained in Ref. 8 by solving mean-field HF equations with the relativistic SO interaction. For the $Pbnm$ phase of YMnO₃, it yields $\phi_2 = 60^\circ$ and $\phi_4 = 240^\circ$. Then, using the value $P_E^{\text{el}} = -0.85 \mu\text{C}/\text{cm}^2$, obtained in the DE limit (see Fig. 2), P^{el} can be estimated as $-0.43 \mu\text{C}/\text{cm}^2$, which is consistent reasonably well with $P^{\text{el}} = -0.55 \mu\text{C}/\text{cm}^2$, obtained for the noncollinear magnetic ground state of YMnO₃ without additional approximations.⁸ In fact, the main discrepancy is caused by the DE limit for P_E^{el} . For example, if one uses $P_E^{\text{el}} = -1.04 \mu\text{C}/\text{cm}^2$, obtained without the DE approximation,⁸ and the angular dependence of \mathbf{P}^{el} , given by Eq. (20), P^{el} can be estimated as $-0.50 \mu\text{C}/\text{cm}^2$, which is much closer to $P^{\text{el}} = -0.55 \mu\text{C}/\text{cm}^2$.

D. Relative directions of electronic and ionic polarization, and problems of structural optimization in LDA+ U

So far, we considered only electronic polarization, which was induced by the orbital ordering in the FM zigzag chains. In this section, we will discuss how this electronic part is

related to the ionic polarization in the noncentrosymmetric $P2_1nm$ structure.

Moreover, we will elucidate the microscopic origin of the “order of magnitude difference”, which typically exists between experimental and theoretical values of the FE polarization, reported for the orthorhombic manganites with twofold periodic magnetic texture. The problem is formulated as follows. The great advantage of the first-principles calculations is that they allow us to perform the structural optimization and to find theoretically the atomic displacements, which are caused by the exchange-striction effects in the E -type AFM phase. If one does such structural optimization for the orthorhombic manganites and subsequently calculates the FE polarization, the latter will be of the order of several $\mu\text{C}/\text{cm}^2$.⁵ The conclusion is rather generic and was obtained for several popular types of the exchange-correlation functionals, such as LSDA (Ref. 8), generalized gradient approximation (GGA, Refs. 5 and 18), and LDA(GGA)+ U (Refs. 5 and 8). The experimental polarization is typically smaller than $0.5 \mu\text{C}/\text{cm}^2$.² On the other hand, if one takes the experimental $P2_1nm$ structure and calculates the FE polarization, it will be at least of the same order of magnitude as the experimental one.^{8,17} The reason of such discrepancy is that, in the experimental $P2_1nm$ structure, there is a large cancelation of electronic and ionic contributions to the FE polarization, while in the theoretically optimized structure, these two contributions have the same sign and the cancelation does not occur.⁸

In this section, we will further clarify the situation. In orthorhombic manganites, there are three types of atomic displacements, which control the FE polarization:

- (i) The Jahn-Teller distortion, which gives rise to the orbital ordering;
- (ii) The exchange striction, which specifies the type of the ordering in the FM zigzag chain and, therefore, the sign of the electronic polarization. Note, that in the centrosymmetric $Pbnm$ structure, the FM chains with the $3x^2-r^2/3y^2-r^2$ and $3y^2-r^2/3x^2-r^2$ type of the orbital ordering are equivalent as they build two degenerate magnetic states. This degeneracy is lifted in the $P2_1nm$ phase by the exchange striction effects, which pick up only one type of the FM zigzag chains (characterized by larger Mn-Mn distances). As soon as the FM chains are selected, the type of the orbital ordering is fixed, so as the sign of the electronic polarization.
- (iii) The FE atomic displacements, which occur in response to the magnetic inversion symmetry breaking and control the sign of the ionic polarization.

The goal of this section is to understand how these three types of the lattice distortions correlate with each other in the experimental and theoretically optimized $P2_1nm$ structures of YMnO_3 .

Let us consider the ionic polarization and concentrate on the behavior of the oxygen sites, which are located in the \mathbf{ab} plane and give the largest contribution to $\mathbf{P}_E^{\text{ion}}$.⁸ In principles, one can consider the contributions of other atomic sites, which do not alter the conclusions. Then, $\mathbf{P}_E^{\text{ion}}$ can be presented in the following form:

$$\mathbf{P}_E^{\text{ion}} = \frac{1}{2V} \sum_i Z_i \Delta \boldsymbol{\tau}_i, \quad (23)$$

where Z_i are the atomic charges and $\Delta \boldsymbol{\tau}_i$ are the atomic displacements away from the centrosymmetric positions. Moreover, it is understood that around each Mn site in the primitive cell, the summation runs over four oxygen sites, located in the nearest neighborhood of Mn. Since each oxygen is shared by two Mn atoms, this leads to the additional prefactor $1/2$. There are many possibilities for choosing the centrosymmetric reference point for evaluation of $\Delta \boldsymbol{\tau}_i$. The final result should not depend on this choice. For our purposes, it is convenient to choose $\Delta \boldsymbol{\tau}_i = \boldsymbol{\tau}_{\text{O}} - \boldsymbol{\tau}_{\text{Mn}}$ (in the other words, we assume that in the centrosymmetric structure, all oxygen sites “fall” on the central Mn site). This can be done because Mn sites do not contribute to the FE polarization of the ionic type along the orthorhombic \mathbf{a} axis.⁸ The reason is that, apart from a constant shift, the projections of Mn sites onto the \mathbf{a} axis are either 0 or $a/2$ (modulo the lattice translation a) and, therefore, can be transformed to each other by the reflection $a \rightarrow -a$. The Mn sites do contribute to the ionic polarization in the \mathbf{bc} plane. However, all these contributions have antiferroelectric character and cancel out after summation over the primitive cell. Thus, around each Mn site, the evaluation of $\mathbf{P}_E^{\text{ion}}$ is reduced to the summation of $\Delta \boldsymbol{\tau}_i$ over neighboring Mn-O bonds with the prefactors given by Eq. (23). Such a construction is very convenient, because in the centrosymmetric $Pbnm$ structure, each Mn site is located in the inversion center. Therefore, the sum of $\Delta \boldsymbol{\tau}_i$ over all neighboring Mn-O bonds will be equal to zero. In the $P2_1nm$ structure, however, such a construction will give us a finite vector, which can serve as a measure of noncentrosymmetric atomic displacements around each Mn site. For our purposes, only the FE (\mathbf{a}) components of these vectors are important, while the \mathbf{b} and \mathbf{c} components are antiferroelectric and will cancel each other. Using this construction and taking the ionic value $Z_{\text{O}} = -2|e|$, the contribution of the planar oxygen sites to P_E^{ion} in the experimental $P2_1nm$ structure can be

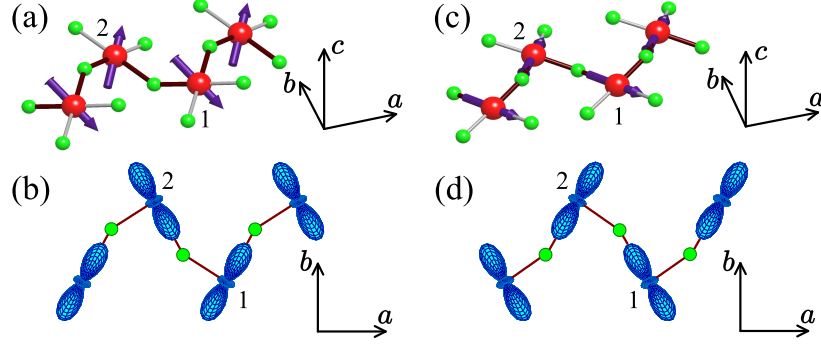


FIG. 9. (Color online) Directions of ionic contributions to the polarization, caused by ferroelectric displacements of oxygen atoms around each Mn site in the ab plane of noncentrosymmetric $P2_1nm$ phase of YMnO_3 (a and c), and the orbital ordering, realized in the ferromagnetic zigzag chain (b and d), as obtained for the experimental (a and b) and theoretically optimized structure (c and d).

estimated as $0.73 \mu\text{C}/\text{cm}^2$, which is totally consistent with the previous finding.⁸

The distributions of such vectors, obtained for the experimental and theoretical structures of YMnO_3 , are shown in Figs. 9(a) and 9(c), respectively. As for the theoretically optimized structure, we use results of LDA+ U calculations with $U = 2.2$ eV (see Ref. 8). Nevertheless, we would like to emphasize that very similar results were obtained in LSDA and LDA+ U with $U = 6.0$ eV.⁸ As is seen in Fig. 9, the FE displacements have the same direction in the experimental and theoretically optimized $P2_1nm$ structure of YMnO_3 . This direction corresponds to the positive value of P_E^{ion} .

Corresponding orbital ordering, realized in the FM chains, is shown in Figs. 9(b) and 9(d), for the experimental and theoretical structure, respectively. For the experimental $P2_1nm$ structure, the orbital ordering is of the $3x^2-r^2/3y^2-r^2$ type. Therefore, the electronic polarization is negative, and there is a partial cancelation of the electronic and ionic terms, which explains a relatively small value of the experimental polarization.⁸ However, the theoretical optimization of the crystal structures, performed both in LSDA and LDA+ U , yields different type of the orbital ordering: $3y^2-r^2/3x^2-r^2$ instead of $3x^2-r^2/3y^2-r^2$. Therefore, the electronic polarization will be positive, and the cancelation does not occur.

Thus, the directions of FE displacements, obtained in LSDA and LDA+ U , are inconsistent with the type of the orbital ordering, realized in the FM zigzag chains. This seems to be a serious problem of the first-principles calculations and at the present stage it is not clear

how it should be solved. On the computational side, many attention recently is paid to the screened hybrid functionals (see, e.g., Ref. 28). Therefore, it would be interesting to see how these functionals will work for the structural optimization in multiferroic compounds, where the inversion symmetry is broken by the magnetic degrees of freedom. The first applications for HoMnO_3 seem to show that the problem persists: although the electronic polarization is decreased, mainly due to the increase of the on-site level splitting, it has the same sign as the ionic one and the total polarization is overestimated in comparison with the experiment.²⁹ On the other hand, the directions of FE displacements can be controlled by the relativistic SO interaction, which is typically ignored in the process of structural optimization. This point of view was proposed, for example, in Ref. 30.

E. Switching electric polarization by changing the magnetic texture

What is interesting about the multiferroic systems is that the value and the direction of the FE polarization depend on the magnetic texture and, by changing this texture, one can also change the vector of polarization. In this section, we will discuss how such a behavior can be realized in the twofold periodic magnetic texture. Again, let us consider the centrosymmetric $Pbnm$ structure and assume that the inversion symmetry is broken exclusively by the magnetic order. In such a case, most of attention is focused on the E -type AFM phase (Fig. 2), which breaks the inversion symmetry but preserves the symmetry operation $\{\hat{C}_a^2|\mathbf{a}/2+\mathbf{b}/2\}$. Therefore, the FE polarization will be parallel to the \mathbf{a} axis.

Now, the question is whether there are other types of the magnetic texture, which would break the inversion symmetry. As an example, let us consider the magnetic texture in Fig. 10(a). In the plane $z = 0$, it is identical to the E -type AFM order, and can be transformed to itself by applying the symmetry operation $\{\hat{C}_a^2|\mathbf{a}/2+\mathbf{b}/2\}$ around even magnetic sites 2 and 4. Alternatively, one can apply the symmetry operation $\{\hat{C}_a^2|-\mathbf{a}/2-\mathbf{b}/2\}$ around odd magnetic sites 1 and 3. In the E -phase, the same symmetry operations can be applied in the planes $z = \pm c/2$ and also will transform the plane $z = c/2$ to the equivalent to it plane $z = -c/2$. The magnetic texture in Fig. 10(a) is obtained by the additional inversion around odd magnetic sites in the plane $z = c/2$, which interchanges the symmetry operations $\{\hat{C}_a^2|\mathbf{a}/2+\mathbf{b}/2\}$ and $\{\hat{C}_a^2|-\mathbf{a}/2-\mathbf{b}/2\}$. Thus, the plane $z = c/2$ can be transformed to itself by the symmetry operation $\{\hat{C}_a^2|\mathbf{a}/2+\mathbf{b}/2\}$ around odd sites or by $\{\hat{C}_a^2|-\mathbf{a}/2-\mathbf{b}/2\}$

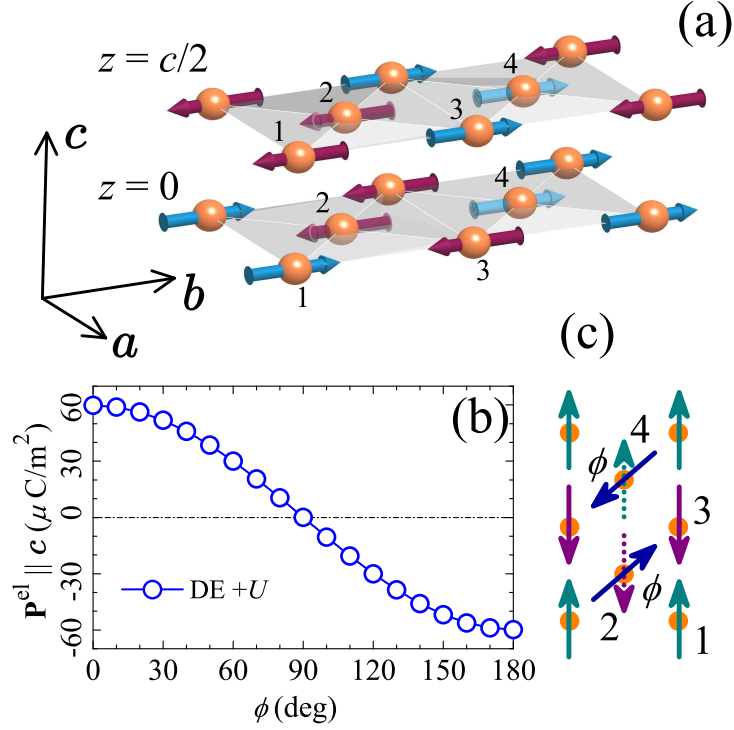


FIG. 10. (Color online) (a) Antiferromagnetic texture yielding finite ferroelectric polarization along the c axis. (b) Behavior of electronic polarization in YMnO_3 upon rotation of magnetic moments, as obtained in the double exchange model with the Hartree-Fock potential $\hat{\mathcal{V}}_i^\dagger$ (DE + U). In the rotated texture, the directions of spins at the sites 1 and 3 were fixed, while the spins at the sites 2 and 4 were rotated by the angle ϕ , as explained in panel (c). The interlayer coupling was kept AFM for the sites 1 and 3 and FM for the sites 2 and 4.

around even sites. Therefore, the symmetry operations $\{\hat{C}_a^2 | \mathbf{a}/2 + \mathbf{b}/2\}$ and $\{\hat{C}_a^2 | -\mathbf{a}/2 - \mathbf{b}/2\}$, although preserved locally in each of the plane, are broken globally, because they cannot simultaneously transform the planes $z = 0$ and $z = \pm c/2$ to themselves.

Instead, the magnetic texture in Fig. 10(a) obeys the symmetry operation $\{\hat{C}_c^2 | \mathbf{c}/2\}$, which is another symmetry operation of the space group $Pbnm$. Therefore, the FE polarization in this phase will be parallel to the c axis. According to the above arguments, each plane may carry a finite polarization parallel to the a axis. However, since neighboring planes are connected by the symmetry operation $\{\hat{C}_c^2 | \mathbf{c}/2\}$, the contributions from different planes will cancel each other.

The behavior of $\mathbf{P} \parallel \mathbf{c}$, obtained in the DE model for YMnO_3 , is explained in Fig. 10(b).

Here, we again consider a continuous rotation of spins between two kinds of the AFM domains via an intermediate spin-spiral phase, as explained in Fig. 10(c). In comparison with Fig. 2, the planes $z = 0$ and $z = c/2$ are connected by the FM pathes between even magnetic sites.

$\mathbf{P}||\mathbf{c}$ appears to be about two orders of magnitude weaker than $\mathbf{P}||\mathbf{a}$ in the E -phase (Fig. 2). Nevertheless, this result is very natural and can be easily understood by considering the perturbation theory arguments, similar to the ones in Sec. III C. Namely, in order to obtain $\mathbf{P}||\mathbf{c}$, we should consider the transfer integrals \hat{t}_{ij} between all possible combinations of sites i and j along the \mathbf{c} axis. Of course, the main contribution is expected from the NN sites. Moreover, according to Eq. (22), in order to contribute to $\mathbf{P}||\mathbf{c}$, these transfer integrals should have both symmetric and antisymmetric components. However, due to the combination of $\{\hat{C}_c^2|\mathbf{c}/2\}$ and the inversion symmetry around the Mn sites, the NN integrals between the planes $z = 0$ and $z = c/2$ will satisfy the following property: $\hat{R}_c^2 \hat{t}_{ij} (\hat{R}_c^2)^T = \hat{t}_{ji}$, where the matrix transformation \hat{R}_c^2 , corresponding to the 180° rotation around the \mathbf{c} axis, changes the sign of some of the matrix elements of \hat{t}_{ij} . Therefore, in the crystal-field representation, one can always choose the phases of the basis orbitals such that the corresponding matrix of the transfer integrals \hat{t}_{ij} would become totally symmetric. Thus, the NN contributions to $\mathbf{P}||\mathbf{c}$ in the second order of $1/\Delta$ will vanish, and $\mathbf{P}||\mathbf{c}$ has finite value due to either next-NN integrals, which are small (all transfer integrals for YMnO_3 can be found in the Supplemental Material of Ref. 8) or the higher-order effects with respect to $1/\Delta$, which are also small. This naturally explains the fact that $\mathbf{P}||\mathbf{c}$ is much smaller than $\mathbf{P}||\mathbf{a}$.

This finding resembles the behavior of multiferroic manganites with nearly fourfold periodic magnetic texture, for which the possibility of switching the electric polarization was demonstrated experimentally.^{2,3} For example, in TbMnO_3 the polarization is aligned along the orthorhombic \mathbf{c} axis. However, the external magnetic field applied along the \mathbf{b} axis will change the magnetic texture and align the polarization parallel to the \mathbf{a} axis.³ Moreover, most of experimental data also confirm the fact that $\mathbf{P}||\mathbf{c}$ is smaller than $\mathbf{P}||\mathbf{a}$. For example, such a behavior is typical for the $\text{Eu}_{1-x}\text{Y}_x\text{MnO}_3$ compounds, containing only non-magnetic rare-earth elements, that excludes the influence of the $4f$ magnetism on the FE polarization.^{2,31} The results of this section suggest that this behavior is more generic and can be anticipated in other regimes, including the twofold periodic magnetic systems. The origin of this phenomenon is related to the specific symmetry of the crystal structure (in

the case of orthorhombic manganites – the $Pbnm$ symmetry) and how it is lowered by the magnetic ordering in the DE limit. It should not be confused with the spin-spiral alignment, which does break the inversion symmetry of the DE Hamiltonian (see Sec. III C).

It is interesting to note that the magnetic texture depicted in Fig. 10 can be viewed as a “defected E -type AFM texture”, where the “defects” are two FM bonds between the planes $z = 0$ and $z = c/2$. Of course, such “defects” are energetically unfavorable and, after including the SO interaction, this magnetic texture will change in order to minimize the FM coupling in the defected bonds. This will lead to the substantial deformation of the magnetic texture in Fig. 10(a). Nevertheless, we would like to emphasize that the noncollinear magnetic texture with $\mathbf{P} \parallel \mathbf{c}$ can be stabilized even after including the SO interaction. The situation was discussed in Ref. 7.

IV. DISCUSSIONS AND CONCLUSIONS

This work is a continuation of previous studies, devoted to multiferroic manganites, which crystallize in the orthorhombic $Pbnm$ and $P2_1nm$ structure.^{7,8} Our main motivation was to present a transparent physical picture, which would explain why and how the ferroelectric polarization is induced by some complex magnetic order. For these purposes we invoke the double exchange theory, which was formulated for the low-energy model, derived from the first-principles electronic structure calculations. As far as the polarization is concerned, the DE theory is very robust and reproduces results of more general mean-field Hartree-Fock calculations at a good quantitative level. Furthermore, the main advantage of the DE theory is that it allows us to greatly simplify the problem and, in a number of cases, derive an analytical expression for the FE polarization. Thus, we could clarify very basic aspects of the FE activity in manganites with twofold periodic magnetic texture.

In our analysis we started from the general Berry-phase theory.^{10,11} In the case of improper ferroelectrics, the basic quantity to be considered is the electronic polarization, which incorporates the change of the electronic structure in response to the noncentrosymmetric alignment of spins. Then, our main message is that, for the analysis of electronic polarization in realistic manganites, one can always use two physical limits. The first one is the limit of large intra-atomic splitting Δ_{ex} between the majority- and minority-spin states. The second one is the limit of large intra-atomic splitting Δ between the majority-spin e_g

states. Therefore, for the electronic polarization, one can always consider the perturbation theory expansion with respect to both $1/\Delta_{\text{ex}}$ and $1/\Delta$. This perturbation theory describes asymmetric transfer of some weight of the Wannier functions to the neighboring sites, which gives rise to the polarization.

There is some similarity with the theory of superexchange interactions, which deals with the virtual hoppings,¹² and where the terms proportional to $1/\Delta$ and $1/\Delta_{\text{ex}}$ account for the FM and AFM contributions, respectively.¹³ Therefore, the DE limit $\Delta_{\text{ex}} \rightarrow \infty$ would correspond to neglecting all AFM contributions. It may not be a good approximation for interatomic magnetic interactions. Nevertheless, the main difference for the electronic polarization is that it appears only in the second order with respect to $1/\Delta$ and $1/\Delta_{\text{ex}}$. The physically relevant picture corresponds to the situation where $\Delta_{\text{ex}} > \Delta$. Then, due to the inequality $(\Delta/\Delta_{\text{ex}})^2 \ll \Delta/\Delta_{\text{ex}}$, it is logical to keep the effects of the first order of $1/\Delta_{\text{ex}}$ in the analysis of superexchange interactions, but neglect the effects of the second order of $1/\Delta_{\text{ex}}$ in the analysis of electronic polarization. This again justifies the use of the DE limit in the latter case.

On the basis of this perturbation theory expansion, we were able to explain how the electronic polarization depends on the relative directions of spins in an arbitrary twofold periodic magnetic texture. Particularly, the multiferroic effect in orthorhombic manganites is a nonlocal phenomenon in the sense that the inversion symmetry is broken by making some of the Mn-Mn bonds magnetically inequivalent. In the DE model, this inequivalence is achieved by the additional modulation of transfer integrals by ξ_{ij} . Then, one trivial conclusion is that there will be no magnetic inversion symmetry breaking in the spin-spiral phase, where all ξ_{ij} are the same. Therefore, in order to make finite polarization, it is essential to deform the spin spiral. In orthorhombic manganites, such deformation is caused by the relativistic spin-orbit interaction.^{7,8} The second important precondition for the FE activity is the asymmetry of the transfer integrals, which should simultaneously have symmetric and antisymmetric components.

We also pointed out on a serious problem in the structural optimization, which apparently exists in the first-principles calculations (at least at the level of LDA+ U and GGA+ U approximations for the exchange-correlation functional without relativistic spin-orbit coupling) and which typically results in the large overestimation of the value of FE polarization in comparison with experimental data.⁸ In this work, we were able to clarify the origin

of this problem: in the theoretical structure, the directions of noncentrosymmetric atomic displacements are inconsistent with the type of the orbital ordering in the ferromagnetic zigzag chains, which controls the sign of the electronic polarization. As the result, the electronic and ionic contributions have the same sign in the theoretically optimized structure, while, according to the experimental crystal structure, they should have opposite signs and partially cancel each other.

Finally, we explained how the electronic polarization can be switched between orthorhombic ***a*** and ***c*** directions by inverting the magnetic texture in every second ***ab*** plane. We also expect a gigantic change of the absolute value of the polarization itself, which is related to very different symmetry properties of the nearest-neighbor transfer integrals along the ***c*** direction and in the ***ab*** plane of manganites.

In this work, our analysis was limited by twofold periodic magnetic textures, which illustrate the basic idea of the double exchange theory of ferroelectric polarization. The idea can be extended to the systems with more general magnetic periodicity: apart from the additional complexity of the magnetic texture, there is no fundamental difference between twofold and more general magnetic periodicity. In both cases, the basic property, which should be considered and which gives rise to the ferroelectric activity is the alternation of angles between spins in different Mn-Mn bonds.

Acknowledgements. This work is partly supported by the grant of the Ministry of Education and Science of Russia N 14.A18.21.0889.

* SOLOVYEV.Igor@nims.go.jp

¹ Y. Tokura, Science **312**, 1481 (2006); T. Kimura, Annu. Rev. Mater. Res. **37**, 387 (2007); S.-W. Cheong and M. Mostovoy, Nature Materials **6**, 13 (2007); D. Khomskii, Physics **2**, 20 (2009).

² S. Ishiwata, Y. Kaneko, Y. Tokunaga, Y. Taguchi, T. Arima, and Y. Tokura, Phys. Rev. B **81**, 100411 (2010).

³ T. Kimura, T. Goto, H. Shintani, K. Ishizaka, T. Arima, and Y. Tokura, Nature **426**, 55 (2003); T. Kimura, G. Lawes, T. Goto, Y. Tokura, and A. P. Ramirez, Phys. Rev. B **71**, 224425 (2005).

⁴ I. A. Sergienko, C. Şen, and E. Dagotto, Phys. Rev. Lett. **97**, 227204 (2006).

⁵ S. Picozzi, K. Yamauchi, B. Sanyal, I. A. Sergienko, and E. Dagotto, Phys. Rev. Lett. **99**,

- 227201 (2007).
- ⁶ H. Katsura, N. Nagaosa, and A. V. Balatsky, Phys. Rev. Lett. **95**, 057205 (2005); M. Mostovoy, *ibid.* **96**, 067601 (2006); I. A. Sergienko and E. Dagotto, Phys. Rev. B **73**, 094434 (2006).
 - ⁷ I. V. Solovyev, Phys. Rev. B **83**, 054404 (2011).
 - ⁸ I. V. Solovyev, M. V. Valentyuk, and V. V. Mazurenko, Phys. Rev. B **86**, 144406 (2012).
 - ⁹ M. Mochizuki, N. Furukawa, and N. Nagaosa, Phys. Rev. Lett. **105**, 037205 (2010).
 - ¹⁰ R. D. King-Smith and D. Vanderbilt, Phys. Rev. B **47**, 1651 (1993); D. Vanderbilt and R. D. King-Smith, *ibid.* **48**, 4442 (1993).
 - ¹¹ R. Resta, J. Phys.: Condens. Matter **22**, 123201 (2010).
 - ¹² P. W. Anderson, Phys. Rev. **115**, 2 (1959).
 - ¹³ K. I. Kugel and D. I. Khomskii, Sov. Phys. Usp. **25**, 231 (1982).
 - ¹⁴ C. Zener, Phys. Rev. **82** 440 (1951); P. W. Anderson and H. Hasegawa, Phys. Rev. **100** 675 (1955); P.-G. de Gennes, Phys. Rev. **118** 141 (1960); K. Kubo and N. Ohata, J. Phys. Soc. Jpn. **33** 21 (1972).
 - ¹⁵ I. V. Solovyev, J. Phys.: Condens. Matter **20**, 293201 (2008).
 - ¹⁶ I. Solovyev, J. Phys. Soc. Jpn. **78**, 054710 (2009).
 - ¹⁷ D. Okuyama, S. Ishiwata, Y. Takahashi, K. Yamauchi, S. Picozzi, K. Sugimoto, H. Sakai, M. Takata, R. Shimano, Y. Taguchi, T. Arima, and Y. Tokura, Phys. Rev. B **84**, 054440 (2011).
 - ¹⁸ K. Yamauchi, F. Freimuth, S. Blügel, and S. Picozzi, Phys. Rev. B **78**, 014403 (2008).
 - ¹⁹ P. Barone, K. Yamauchi, and S. Picozzi, Phys. Rev. Lett. **106**, 077201 (2011).
 - ²⁰ I. V. Solovyev and K. Terakura, Phys. Rev. Lett. **83**, 2825 (1999); I. V. Solovyev, Phys. Rev. B **63**, 174406 (2001).
 - ²¹ J. Kanamori, J. Appl. Phys. **31**, 14S (1960).
 - ²² J. C. Slater and G. F. Koster, Phys. Rev. **94**, 1498 (1954).
 - ²³ X. L. Qi, T. L. Hughes, and S.-C. Zhang, Phys. Rev. B **78**, 195424 (2008).
 - ²⁴ T. Hotta, M. Moraghebi, A. Feiguin, A. Moreo, S. Yunoki, and E. Dagotto, Phys. Rev. Lett. **90**, 247203 (2003).
 - ²⁵ For $\Delta=0$, the integral (15) can be evaluated analytically: note that $\int_0^{2\pi/a} dk = \int_0^{\pi/a} dk + \int_{\pi/a}^{2\pi/a} dk$, and use that $\int_{\pi/a}^{2\pi/a} dk$ can be further transformed to $\int_0^{\pi/a} dk$ after replacing $d_z(k)$ by $-d_z(k)$.
 - ²⁶ J. Zak, Phys. Rev. Lett. **62**, 2747 (1989).

- ²⁷ A. Muñoz, M. T. Casáis, J. A. Alonso, M. J. Martínez-Lope, J. L. Martínez, and M. T. Fernández-Díaz, *Inorg. Chem.* **40**, 1020 (2001).
- ²⁸ J. He and C. Franchini, *Phys. Rev. B* **86**, 235117 (2012).
- ²⁹ A. Stroppa and S. Picozzi, *Phys. Chem. Chem. Phys.* **12**, 5405 (2010).
- ³⁰ A. Malashevich and D. Vanderbilt, *Phys. Rev. Lett.* **101**, 037210 (2008); *Phys. Rev. B* **80**, 224407 (2009).
- ³¹ K. Noda, M. Akaki, F. Nakamura, D. Akahoshi, and H. Kuwahara, *J. Magn. Magn. Matter.* **310**, 1162 (2007).